Journal of Sound and Vibration 484 (2020) 115540

Contents lists available at ScienceDirect

Journal of Sound and Vibration

journal homepage: www.elsevier.com/locate/jsvi

Aeroacoustics research in Europe: The CEAS-ASC report on 2019 highlights

Roberto Camussi [a], Gareth J. Bennett [b,*]

[a] University of Roma Tre, Department of Engineering, Via Della Vasca Navale 79, 00146 Rome, Italy
[b] Department of Mechanical and Manufacturing Engineering, School of Engineering, Trinity College Dublin, The University of Dublin, D02 PN40, Ireland

ARTICLE INFO

Article history:
Received 21 May 2020
Accepted 19 June 2020
Available online 27 June 2020
Handling Editor: J. Astley

Keywords:
Aeroacoustics
Aviation
Aeronautics

ABSTRACT

The Council of European Aerospace Societies (CEAS) Aeroacoustics Specialists Committee (ASC) supports and promotes the interests of the scientific and industrial aeroacoustics community on a European scale and European aeronautics activities internationally. In this context, "aeroacoustics" encompasses all aerospace acoustics and related areas. Each year the committee highlights some of the research and development projects in Europe.

This paper is a report on highlights of aeroacoustics research in Europe in 2019, compiled from information provided to the ASC of the CEAS. In addition, during 2019, a number of research programmes involving aeroacoustics were funded by the European Commission. Some of the highlights from these programmes are also summarised in this article, as well as highlights from other programmes funded by national programmes or by industry. Furthermore, a concise summary of the CEAS-ASC annual scientific workshop: "New Materials for Applications in Aeroacoustics" held in the University of Roma Tre, Italy in September 2019 is included in this report.

Enquiries concerning all contributions should be addressed to the authors who are given at the end of each subsection.

1. CEAS-ASC workshop

The 23rd edition of the CEAS-ASC workshop was hosted by the Department of Engineering of the Roma TRE University, on September 26–27, 2019, with the title "New materials for applications in aeroacoustics". The workshop was organised by Umberto Iemma (Roma Tre University), who also chaired the scientific committee with the co-chairing support of Roberto Camussi (Roma Tre University). The workshop was co-sponsored by the European H2020 Projects ANIMA (Aviation Noise Impact Management through Novel Approaches) and AERIALIST (AdvancEd aicRaft-noIse-AlLeviation devIceS using meTamaterials), and the America Institute of Aeronautics and Astronautics. The choice of the topic was induced by the substantial increase of the research on innovative materials for noise mitigation during the last decade. This interest was induced by the urgent need of breakthrough technologies and concepts to guarantee a sustainable development of commercial aviation. The advent of new ideas for smart and tuneable materials, metamaterials, and active and passive sound absorption systems, makes this field one of the most effervescent in aviation-related research. This interest was confirmed by more than 50 attendants, with a dense, two-days programme comprising 25 papers presented in five thematic sessions, and four keynote lectures. The first keynote

* Corresponding author.
E-mail address: gareth.bennett@tcd.ie (G.J. Bennett).

https://doi.org/10.1016/j.jsv.2020.115540

of the workshop, entitled "Locally resonant vibro-acoustic metamaterials for compact lightweight noise control engineering solutions", was presented by professor Wim Desmet (KU Leuven) who gave a comprehensive review of the fundamental principles underlying response of metamaterials based on local resonance, completed by an overview of applications of noise and vibration control. The second keynote was given by professor Wonju Jeon (KAIST, South Korea) on "Acoustic Metamaterials and Metasurfaces: Effect of Flow and Visco-thermal Losses". The keynote covered the analysis of the effect of compressibility on the response of a metamaterial for acoustic cloaking, and of visco-thermal losses on metasurfaces for sound absorption, including a final overview on acoustic black-holes. On day two, Dr. Eng. Estelle Piot (ONERA Toulouse) delivered the keynote "Example of advanced identification techniques and design tools applied to innovative aeroacoustic liners," where the most advanced designed strategies for acoustic liners have been illustrated, including the paramount issue of quantification of design and manufacturing uncertainties. Finally, the closing keynote was presented by professor Francesco Asdrubali and entitled "Sustainable materials and metamaterials for acoustical applications." Professor Asdrubali has brought to the workshop audience an interesting, cross-disciplinary experience in the development of sustainable, bio-inspired acoustic materials in the field of civil engineering. The 25 presentations were organised in a scientific programme divided into five technical sessions. Day one started with the two sessions on "Theoretical and numerical modelling", chaired by Lorenzo Burghignoli (Roma Tre University) and John Kennedy (Trinity College Dublin), respectively, with eleven contributions in total. Great attention was dedicated to the metamaterials and metasurfaces with sub-wavelength response, and to the modelling of wall impedance of innovative concepts. The session on "Trailing edge noise mitigation, chaired by Dr. Ing. Lars Enghardt (DLR) has closed day one, with four contribution dealing with the numerical and experimental assessment of porous materials. The second day was opened by the "Manufacturing and experimental assessment" session, chaired by Mahdi Azarpeyvand (University of Bristol). Six paper were presented, providing an overview of all the issues related to the realization and the experimental assessment of innovative materials with unconventional responses. Special attention was paid to the estimate of manufacturing uncertainties. The workshop was close by the session on "Active and tuneable concepts", chaired by Hervé Lissek (EPFL), with four papers presenting new adjustable materials for the mitigation of engine noise exploiting electroacoustic and acoustoelastic multiphysics interactions. The entire program of the workshop and the related presentations are available on https://ceas-asc-workshop-2019.ing.uniroma3.it. It is worth mentioning that the annual meeting of the H2020 project ANIMA, co-sponsor of the workshop, was held in the same location, in parallel to the workshop. This has guaranteed a stimulating, multidisciplinary exchange between the attendees of the two events, promoting a wider dissemination of knowledge and technical achievements. A special issue of the International Journal of Aeroacoustics is in preparation and is expected to be published in summer 2020 (guest editor Lorenzo Burghignoli).

2. Airframe noise

2.1. Physics based approaches to design porous materials for noise reduction

Turbulent boundary layer trailing edge noise and vortex impingement noise can be mitigated using porous or flow permeable materials [1,2] once the hydrodynamic sources and the noise generation mechanisms are characterized in detail at both lab scale [3,4] and full scale for conventional and new configurations, such as the boundary layer ingestion one [5].

Recent studies carried out at Delft University of Technology have shown that design of the flow permeable materials is strongly dependent on the size of the turbulent flow structures and the physical mechanisms behind noise generation.

For the case of turbulent boundary layer trailing edge noise, it has been found noise reduction is generated by mitigation of the impedance mismatch at the trailing edge due to the flow permeable trailing edge [1]. Measurements, with different foams, have shown that in this case the location of the noise source moves upstream of the trailing edge, thus confirming distributed scattering along the porous surface, see Fig. 1. To further reduce noise, it is necessary to mitigate the discontinuity at between the solid and the porous surface opening the way to materials with optimal distribution of porosity.

Differently, for vortex impingement noise either for propeller-wing [2] and rotor stator interaction noise [3,4], the size of the impinging flow structure is relatively large thus making more challenging the design of flow permeable surfaces. Experiments carried out by positioning a pylon in the wake of a propeller [2] have shown that a flow permeable leading edge, realized with a porous surface backed by an empty cavity, is not an optimal solution for noise reduction. In order to study, these noise sources in details a rod-cascade wind tunnel model has been designed using high fidelity numerical simulations and built. This will open the way to explore new noise reduction technologies.

Written by Francesco Avallone: f.avallone@tudelft.nl, *Daniele Ragni and Damiano Casalino, Delft University of Technology, The Netherlands.*

2.2. Noise generation of a circulation control airfoil with Coanda flap and droop nose

Circulation control airfoils are considered as a means to reduce the overall noise of the high lift system on transport aircraft. They can be designed as slit-less systems without slat, which is the main acoustic source on a conventional multi-element high lift system. To achieve high lift coefficients, they may be equipped with a trailing edge plain flap and a droop nose. To avoid flow separation on the flap suction side, a high velocity thin wall parallel blowing is realized directly upstream of the flap. The so-called Coanda-effect was already described in the early 1900s and first patented by Henry Coanda [6]. First experimental results have shown that the noise emission from such an airfoil might be lower than from a conventional slat at similar flight conditions

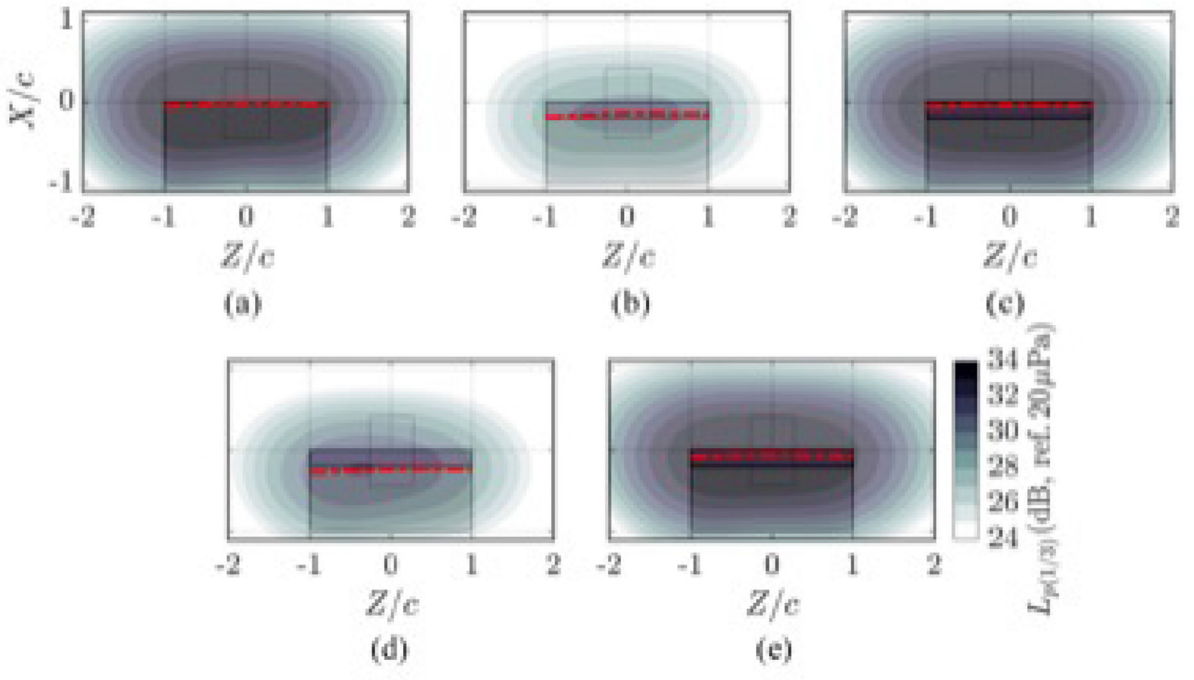

Fig. 1. Source maps for the one-third octave band with $f_c = 1000$ Hz for the measured test cases. (a) Solid. (b) Permeable with 450 μm foam cell diameter. (c) Nonpermeable Permeable with 450 μm foam cell diameter. (d) Permeable with 800 μm foam cell diameter. (e) Nonpermeable Permeable with 800 μm foam cell diameter.

[7]. Furthermore, the achievable high lift coefficient allows for steep flight paths and low speeds, which add to a reduced sound impact on the ground.

Recent numerical investigations based on a hybrid CFD/CAA approach were used to identify the dominant source mechanisms on a circulation control airfoil with flap [8,9]. It was found that three different sources are contributing to the overall noise. These are jet mixing noise at the blowing, curvature noise from the accelerated flow on the flap hinge suction side and trailing edge noise. From these sources, the jet mixing noise was found to be effectively shielded towards the ground due to its location and high frequency, see Fig. 2a. Curvature noise however also contains lower frequencies that are diffracted at the flap trailing edge. Therefore, it is shielded less effectively and contributes as a relevant source to the overall noise imprint on the ground, see Fig. 2b. Trailing edge noise finally also radiates to the lower arc and at similar sound pressure levels as the curvature noise, see Fig. 2c. Therefore, these two sources are considered to be dominant for the overall noise perceived by an observer.

The results of the presented aeroacoustic investigations were obtained within the framework of the German Collaborative Research Center CRC 880, which was completed in 2019 after 9 years. The final results will be published as a book in the first half of 2020.

Written by Lennart Rossian: lennart.rossian@dlr.de, *Roland Ewert, Jan W. Delfs, DLR, Germany*.

2.3. Multi-approach study on nose landing gear noise

The noise emissions of a full-scale nose landing gear (NLG), measured in a wind tunnel and obtained from computational simulations (within the European Clean Sky-funded project ALLEGRA (Advanced Low noise Landing main and nose Gear for Regional Aircraft) [10,11]), were compared with those of three regional aircraft types recorded in flyover measurements under operational conditions in Amsterdam Airport Schiphol [12]. A comparison was also made with the airframe noise prediction models of Fink, Guo, and the German Aerospace Center (DLR). In general, a good agreement was found between all the spectra, see Fig. 3. Overall, hybrid studies as this one are of high interest because they provide different insights that are not obtainable using a single approach and can help to fully understand the noise generation in landing gears. Flyover measurements showed the presence of a strong tonal noise at around 2200 Hz that was not measured in the wind-tunnel experiments, which is likely to be caused by (small) open cavities in the NLG system. This type of noise is perceived as especially annoying but this phenomenon is not accounted for in prediction models. Removing these tones would result in noise reductions of up to 2 dB. On the other hand, wind-tunnel tests allowed for a detailed study of the NLG noise emissions and their scaling at different flow velocities. The noise emissions up to 1.2 kHz were found to scale with the 6th power of the flow velocity, as expected however, the spectra at higher frequencies collapsed better when scaled to the 7th power, confirming the fact that high-frequency noise is radiated from the turbulent flow surrounding small features of the NLG [13]. Measurements with microphone arrays in the wind-tunnel tests and computational simulations showed that the main noise sources were located in the mi ddle of the wheel axle, followed

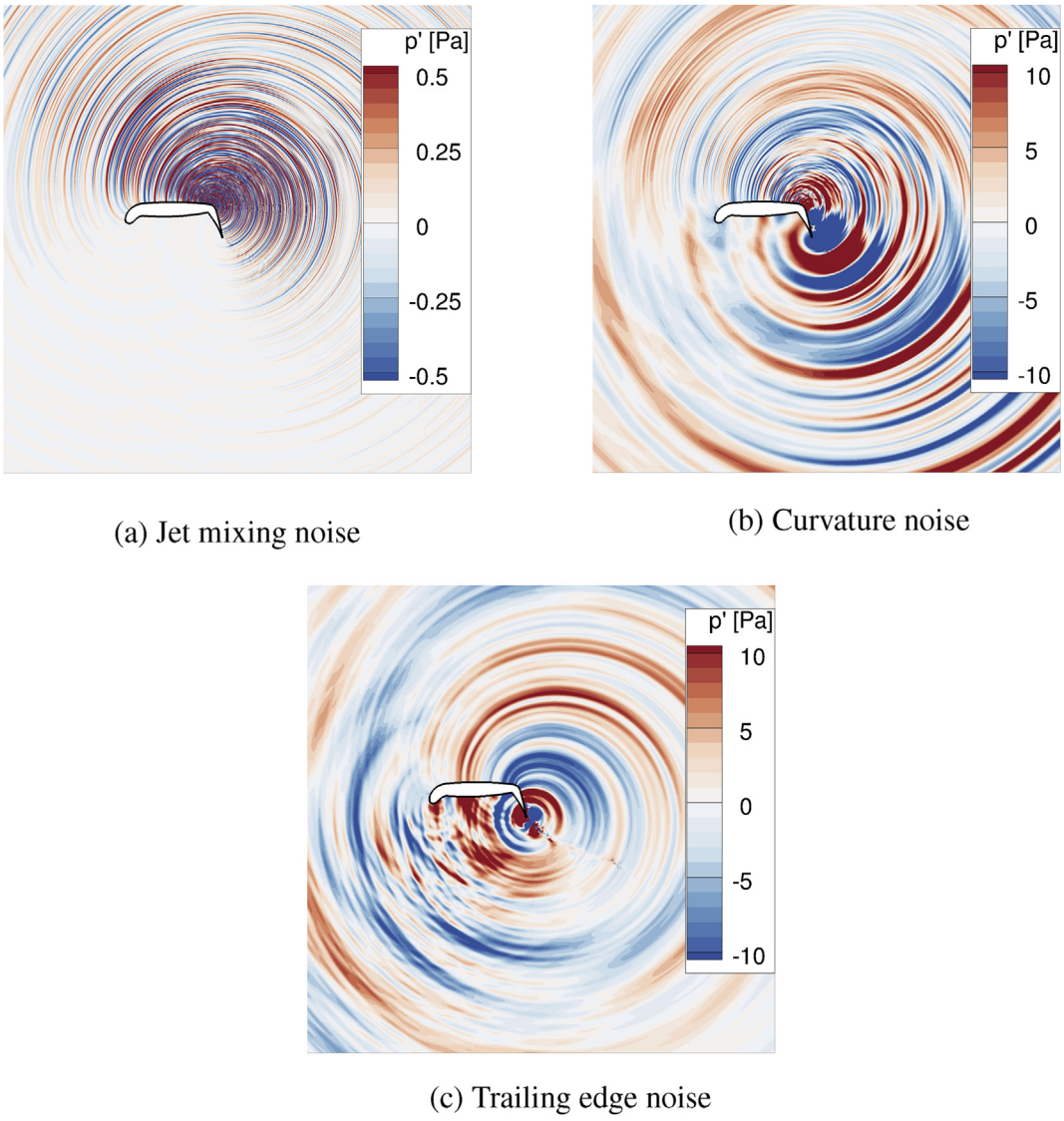

Fig. 2. Snapshop of the acoustic pressure fields.

by the main strut and bay doors, see Fig. 4. Computational simulations allowed for the analysis of emission angles that are not practical in other approaches, such as the upwind direction, see Fig. 4 (right). In general, the use of these three approaches should be combined in order to update and improve the current noise prediction models, that seem to be too simple for detailed studies as this one.

Written by Roberto Merino-Martinez: r.merinomartinez@tudelft.nl, *Delft University of Technology, the Netherlands, and Gareth J. Bennett:* gareth.bennett@tcd.ie, *Trinity College Dublin, the University of Dublin, Ireland.*

2.4. Flyover noise source localization during acoustic flight tests of advanced passenger aircraft

According to the program of preliminary certification flight tests of modern passenger aircraft, localization of noise sources was performed. Thus, simultaneously with the flight tests TsAGI carried out acoustic measurements for localization and ranking of its noise sources with the help of 108-microphone array [14]. The flyovers of the aircraft in approach configuration were performed for various flight altitudes, pitch angles, engine operation modes, and the position of high-lift devices (HLD). Noise source localization maps (see Fig. 5), as well as spectra of the individual source zones were calculated and a ranking of the sources based on the overall sound pressure levels in each source region was obtained. For the aircraft, a large-scale semi-span model of the wing with HLD in approach configuration (see Figs. 6 and 7 was tested in DNW-NWB previously [15]. Comparison of noise spectra due to HLD scaled based on Strouhal number, as well as comparison of localization maps for DNW-NWB and

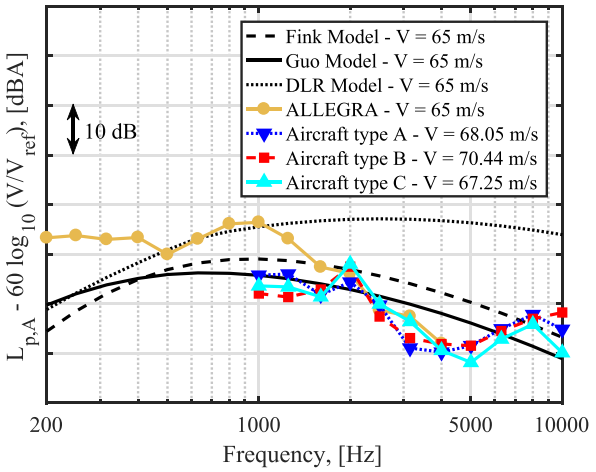

Fig. 3. Comparison of the one-third-octave band A-weighted NLG noise emissions in the flyover direction measured in the wind tunnel (ALLEGRA), flyovers and noise prediction models. Spectra normalized for a reference velocity of 65 m/s [13].

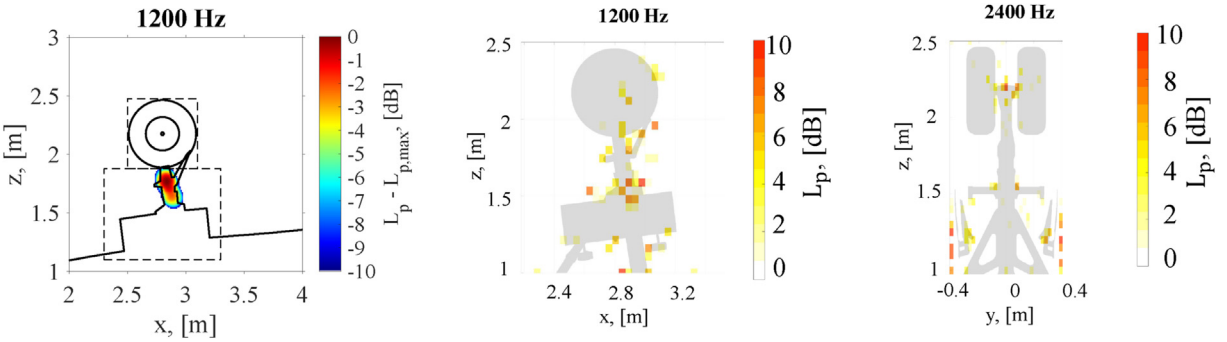

Fig. 4. One-twelfth-octave band acoustic source plots of the ALLEGRA NLG at a flow velocity of 50 m/s. Left: Wind tunnel test on the side direction at 1200 Hz. Center: Computational simulations on the side direction at 1200 Hz. Right: Computational simulations on the front direction at 2400 Hz [13].

flight data demonstrated a reasonably good agreement. The analysis of the flight test results on localizing and ranking the noise sources showed that for the aircraft in the approach configurations, the airframe contributed about the same as the power plant to the total noise of the aircraft.

Written by Mikhail mikhail.y.zaytsev@tsagi.ru, *Victor Kopiev, Ivan Belyaev, TsAGI, Russia.*

3. Fan and jet noise

3.1. Turbofan broadband noise predictions based on a ZDES calculation of a fan-OGV stage

Broadband noise (BBN) generated by rotor-stator interactions is a dominant turbofan source mechanism and its prediction on modern engines is still a challenging task. An hybrid RANS/LES calculation coupled with acoustic analyses have been performed at ONERA in the framework of a European project, TurboNoiseBB. BBN predictions in industry are currently assessed using averaged turbulence information derived by RANS and coupled to semi-analytical models. The numerical approach proposed here relies on a Zonal Detached Eddy Simulation (ZDES) strategy [1] that is applied at approach conditions to a fan module equipped with 20 rotor blades and 44 outlet guide vanes (see Fig. 8) and tested in AneCom facility (Wildau, Germany). Post-processed data are used to feed directly acoustic codes based on Amiet theory and Ffowcs-Williams and Hawkings analogy [2], for which required inputs are the turbulent wake spectral information and the unsteady pressure over the vane wall, respectively. The turbulent wake characteristics in terms of energy and spectral content have been compared to hot-wire measurements (see Fig. 9). In particular radial profiles of turbulent velocity components and power spectrum density (PSD) at selected duct height positions have been analysed, as well as integral and spanwise correlation length scales. Hence, sound power spectra in the bypass duct have been assessed and successfully compared to the experiment (see Fig. 10). This work was funded by European Union's Horizon 2020 research and innovation programme under grant agreement No. 690714.

Written by Cyril Polacsek: cyril.polacsek@onera.fr, *and Benjamin François, Raphael Barrier, Majd Daroukh, ONERA, The French*

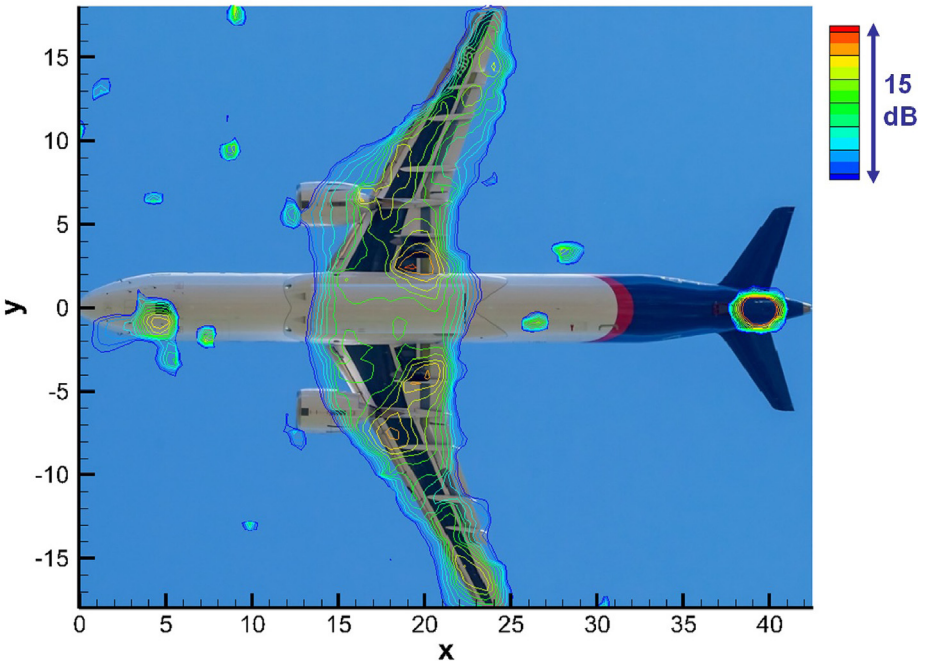

Fig. 5. Example of noise source localization map for aircraft flyover in flight tests.

Fig. 6. Half-span wing model in anechoic test section of DNW-NWB wind tunnel.

Aerospace Lab, FRANCE.

3.2. Experimental investigation of fan broadband noise generation and transmission using sparse sensor arrays

Novel insights into the noise generation and into transmission effects of a large-scale turbo fan model were achieved by application of advanced mode analysis techniques to sparse sensor arrays in the fan inlet, interstage, and bypass duct [16,17]. The measurements were taken at the ACAT1 fan operated in the UFFA test facility of AneCom AeroTest within the EU-project TurboNoiseBB. The implementation of compressed sensing [18] enabled detailed mode analyses providing large dynamic ranges at high frequencies. Unexpectedly strong rotor-coherent modes were detected in the interstage measurements and could be ascribed to rotor wake irregularities. Combinations with inlet respectively bypass measurements revealed the contributions of the rotor and stator bound sources. Compared to the tones, rotor shielding effects were found to be less important for the broadband components that were dominated by rotor co-rotating modes. Analyses of inter-mode coherences evidenced a tunnel effect of cut-off modes through the stator inter-vane channels, which - after scattering into cut-on modes - significantly contribute to the downstream radiated sound field. Full radial mode decomposition of the broadband components was realized

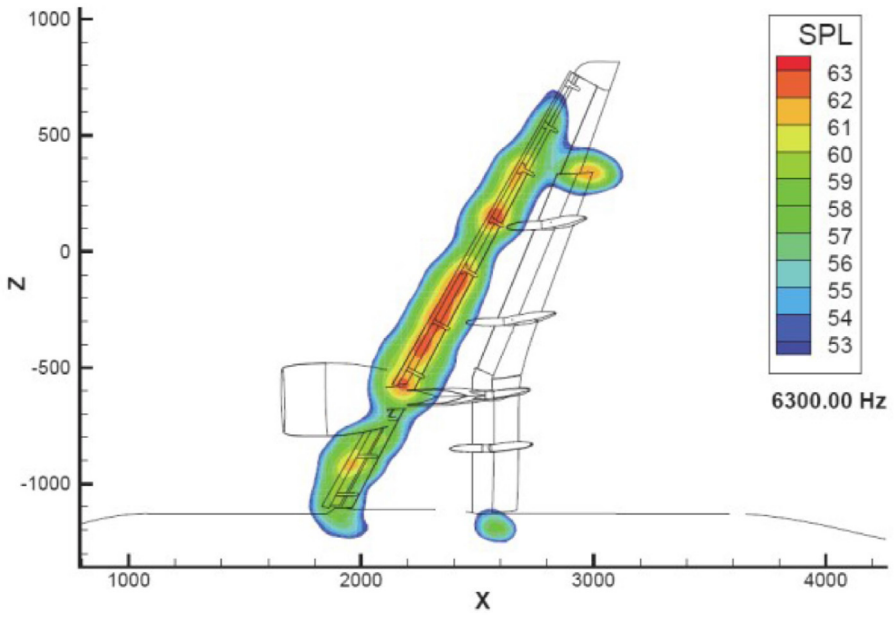

Fig. 7. Example of noise source localization map for DNW-NWB tests.

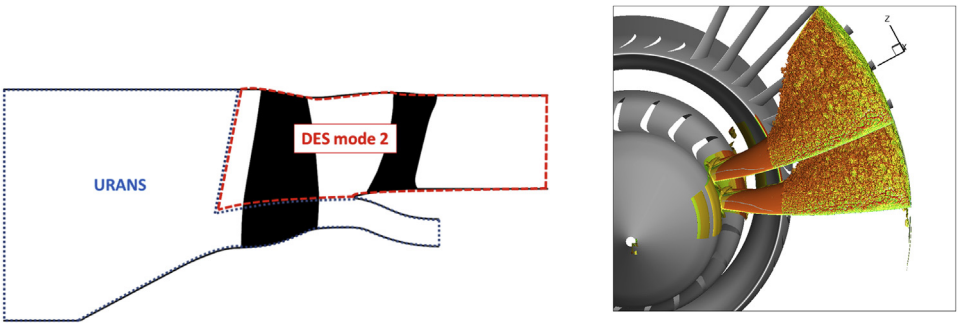

(a) URANS and DES zones.

(b) Iso-value surfaces of the Q criterion around the fan blades.

Fig. 8.

in the bypass using a combined axial and azimuthal sensor array [19], compare Fig. 11. The impact of the axial flow profile on the analysis was considered. The evaluated sound power was compared to the outcome of sound power estimation techniques relying on the azimuthal mode analysis or the axial wave number decomposition, each in combination with the assumption of a specific energy distribution among the radial mode orders, compare Fig. 12. Finally, the comparison questions the general suitability of the 'equal energy per mode' model.

Written by Maximilian Behn: Maximilian.Behn@dlr.de, *Ulf Tapken, Lars Enghardt, DLR, Germany*.

3.3. Study of noise generation by large-scale coherent structures in high-speed jets using conditional averages

Noise generation by large-scale coherent structures has been investigated using numerical simulations of high-speed jets at Mach numbers ranging from 0.3 to 3 and conditional averages. The latter are computed by averaging flow events selected according to a detection criterion so that only coherent features remain. First, this technique has been applied to temporally-developping subsonic jets [20]. This allowed us to reveal the axisymmetric noise component generated in the downstream direction when the shear layers merge at the closing of the potential core. This component does not significantly vary with the Reynolds number and is consistently observed for jets at Mach numbers ranging from 0.3 to 2 [21]. In a second part, conditional averages have been computed to investigate the generation process of the steepened waves associated with the crackle noise component of supersonic jets. For that, two jets at Mach numbers of 2 and 3 and at a Reynolds number of 12,500 were considered [22]. As represented in Fig. 13, the near pressure fields display high-intensity Mach waves with steep variations indicating the

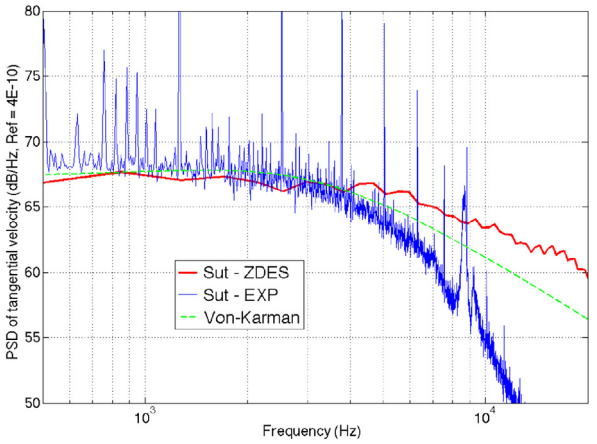

Fig. 9. PSD of upwash velocity at mid-height provided by ZDES and compared to experiment.

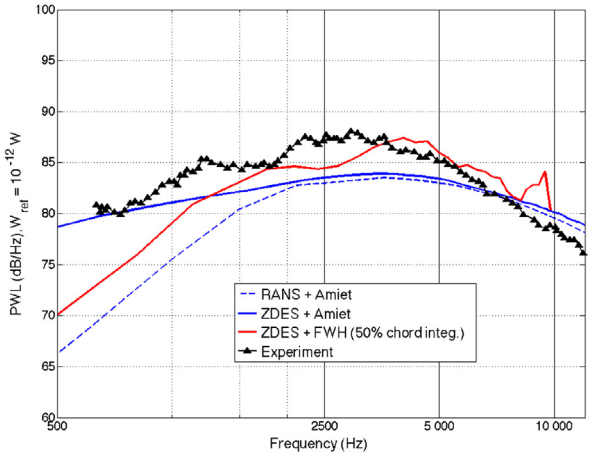

Fig. 10. PWL spectra in the bypass duct assessed by numerical simulations and experiment.

presence of shocks. Using conditional averages such as those displayed in Fig. 14, their generation has been associated with a large-scale vortex located at the lower tip of the pressure waves and convected at a supersonic speed. Finally, the effects of temperature have been investigated [23]. The convection velocity of coherent structures is higher at a higher temperature, leading to stronger and more skewed Mach waves.

Written by P. Pineau: pierre.pineau@ec-lyon.fr, *C. Bogey, École Centrale de Lyon, France.*

3.4. Hybrid LES-RANS of serrated nozzle jets installed under wing

In the pursuit of higher efficiencies, the use of Ultra-High Bypass Ratio (UHBPR) makes aeroengines become installed closer to aircraft wings. This intensifies the sound source produced by the interactions between the propulsive jet and wing. Fig. 15a gives an overview of the jet turbulence and acoustics from an UHBPR engine under a realistic wing. In addition to jet noise, the jet interacts with the wing trailing edge, generating extra acoustics. This composes the majority of installation noise which is faced by UHBPR engines. The interference also occurs at the wing leading edge, scattering the upstream traveling acoustics from the jet. In the EU 7th Framework project JERONIMO, serrations have been designed to mitigate the interactions and hybrid LES-RANS methods have been developed to numerically evaluate serration effects on installation noise reduction from first principles [24]. Serrations introduce streamwise vortices inside the shear layer and significantly increase the mixing near nozzle [25]. The enhanced mixing dissipates turbulent kinetic energy rapidly and decreases the turbulence level when the jet reaches the wing underneath surface, as shown in Fig. 15b. This weakens the jet-wing interactions and hence reduces noise generation. Far-field noise is compared at upstream observer angles where installation noise is more pronounced. Fig. 16 shows that noise prediction for an installed round nozzle agrees with experimental measurements and this is used to verify the hybrid LES-RANS method. The serration nozzle jet was then evaluated using the same method and shows a significant reduction in the peak frequency of

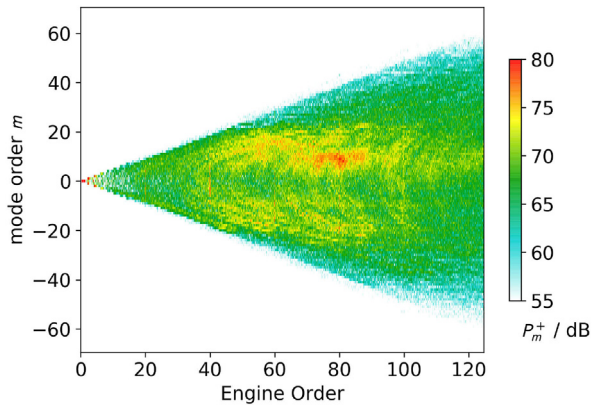

Fig. 11. Broadband noise radiated by ACAT1 fan model into the test rig bypass at approach operating condition. The diagram shows the sound power of each azimuthal mode directly evaluated with a radial mode analysis approach.

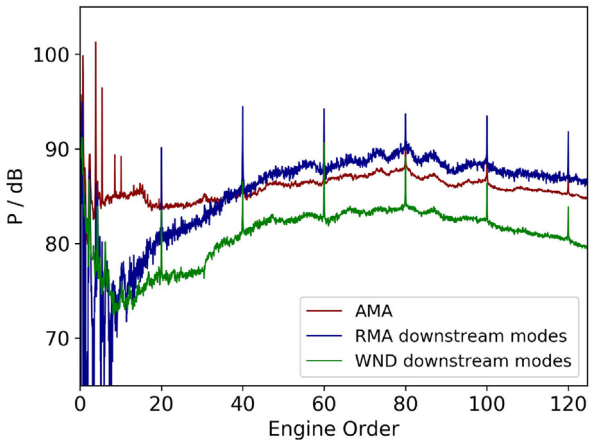

Fig. 12. Overall sound power radiated by the ACAT1 fan. Estimations based on azimuthal mode analysis (AMA) respectively wave number decomposition (WND) in combination with 'equal energy density per mode' model are compared to the radial mode analysis (RMA) result shown in 11.

noise spectra.*Written by Zhong-Nan Wang:* znw22@cam.ac.uk, *James C. Tyacke and Paul G. Tucker, Department of Engineering, the University of Cambridge, UK*.

3.5. Wall-pressure fluctuations induced by a compressible jet flow over a flat plate at different Mach numbers

The introduction of the Ultra-High-Bypass-Ratio (UHBPR) engines leads to a reduction of the overall radiated noise. On the other hand, it increases the interaction between the jet exhaust flow and the aircraft surfaces making more important the study of the vibro-acoustic response of structural panels. This work is targeted towards the experimental characterization of the effect of the Mach number on the wall-pressure fluctuations induced by a compressible subsonic jet over an infinite flat plate, used to simulate the aircraft surfaces. Experiments have been performed in a semi-anechoic environment where a compressible jet facility, whose nozzle diameter (D) was 12 mm, is installed. The inflow conditions were varied in order to investigate five different jet Mach numbers in a range between M = 0.5 and M = 0.9, whereas the radial position of the flat plate was fixed at H/D = 2, thus having a negligible intrusiveness on the aerodynamic field [26,27]. An aerodynamic characterization was performed to confirm this assertion.

The wall-pressure fluctuations acting on the flat plate were measured by a pair of cavity-mounted pressure transducers, providing pointwise pressure signals in the streamwise and in the spanwise directions. A sketch of the experimental setup is shown in Fig. 17a.

The jet Mach number effect on the wall pressure fluctuations field is characterized using statistical and spectral quantities, figuring out a possible scaling law of the autospectra, as reported in the following:

$$PSD(St)_{adm} = \frac{PSD(St) \cdot U_j}{P_{ref} \cdot q \cdot D} \tag{1}$$

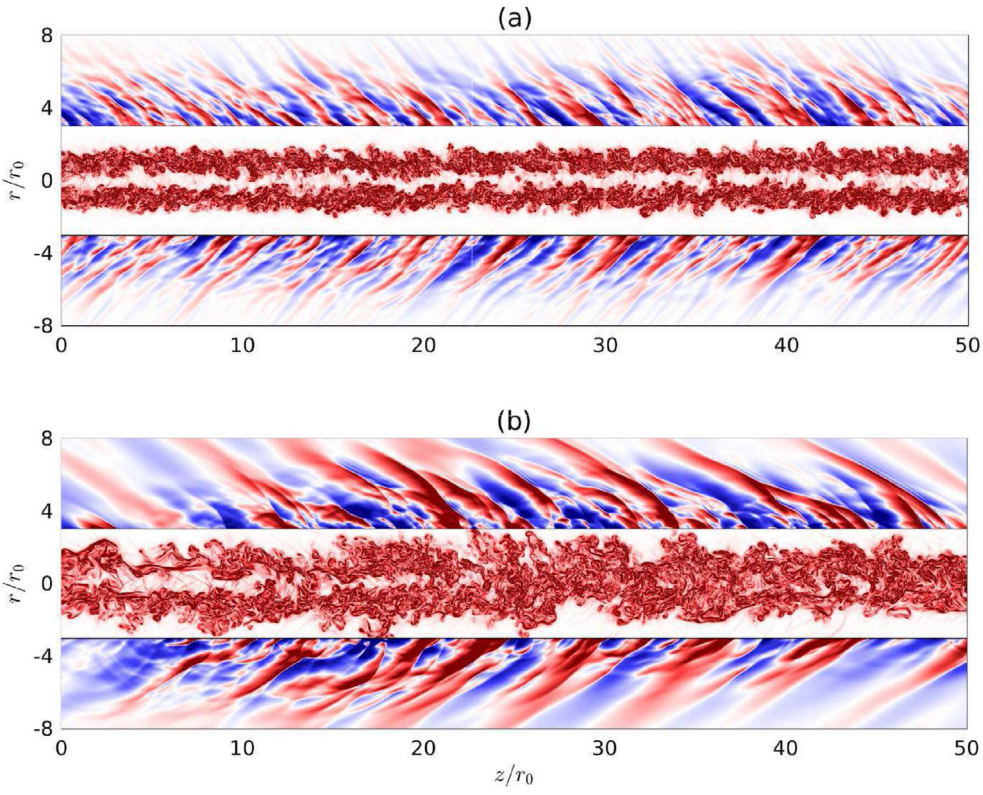

Fig. 13. Snapshots of vorticity and pressure fluctuations for temporally-developing jets at (a) Mach 2 and (b) Mach 3.

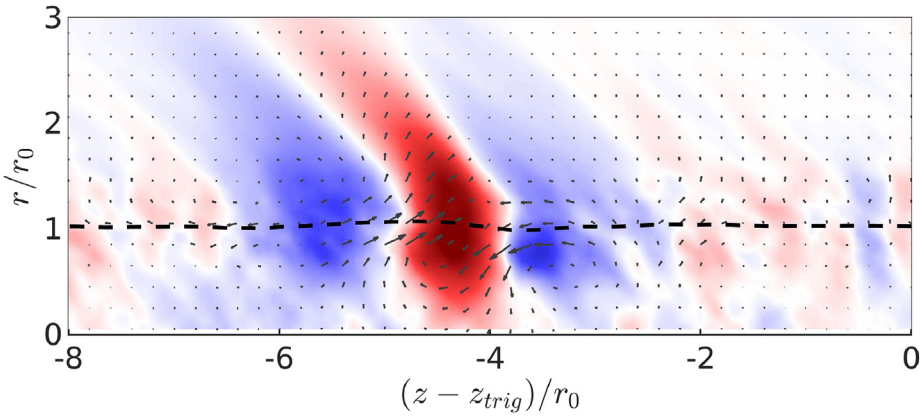

Fig. 14. Conditionally-averaged pressure fluctuations for a temporally-developing Mach 2 jet, with the conditional velocity fluctuations represented as arrows and the conditional sonic line represented as a dashed line. The scale for the pressure ranges from −10000 to 10,000 Pa.

where q is the dynamic pressure, P_{ref} is the reference pressure, U_j is the nozzle exhaust velocity, D is the nozzle exhaust diameter and *PSD* is the power spectral density. An application is reported in Fig. 17b.

Furthermore, implications for wall-pressure fluctuations modelling are also discussed by the application of the Corcos' model, Fig. 18. More results and physical explanations are reported in Ref. [28].

Written by Stefano Meloni: stefano.meloni@uniroma3.it, *Alessandro Di Marco, Matteo Mancinelli, Roberto Camussi, Univeristy of Roma Tre, Italy*.

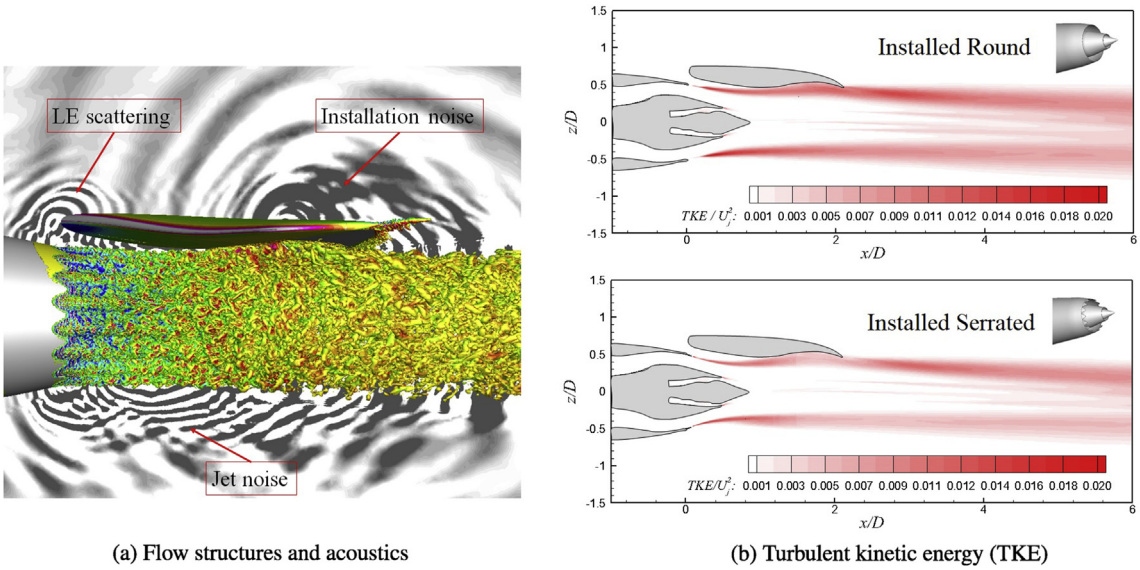

Fig. 15. Installed turbulent jet flows and acoustics.

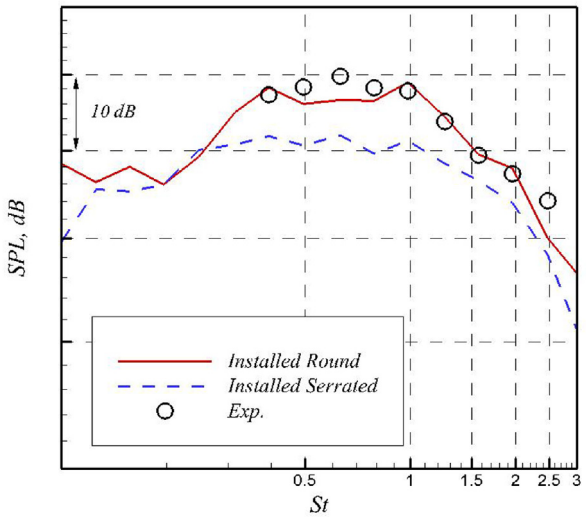

Fig. 16. Installed jet noise sources and far-field sound spectra.

3.6. Azimuthal structure of low-frequency noise of installed jet

In anechoic chamber AC-2 TsAGI, Fig. 19, an experimental study of the azimuthal content of the installed jet noise at low frequencies corresponding to the maximum in installation noise spectra was performed. The azimuthal decomposition technique (ADT) is used to measure azimuthal modes for the isolated and installed jets (i.e. jet near a plate, Fig. 20) at subsonic Mach numbers up to 0.82, without coflow. In the installed configuration, the plate trailing edge is located in the linear hydrodynamic jet near field. It is experimentally demonstrated that jet noise remains practically unaffected by the plate and that installation noise is localized in the azimuthal modes antisymmetric with respect to the plate, which is explained by the dipolar nature of the scattered field leading to the antiphase between the sound fields above and below the plate. A novel procedure of splitting total noise into jet noise and installation noise components is proposed. This enables using only one dataset obtained for the installed configuration to distinguish jet noise and installation noise components. This approach reduces the influence of the experimental errors connected to repeatability of the operating conditions and thus increases the accuracy of the installation noise extraction, especially for high-speed jets at small observation angles where installation noise is masked by the strong jet noise. This procedure allows obtaining quite smooth directivities of the installation noise in a wide range of observation angles not only for low-speed jets but for high-speed jets as well. Comparison of the obtained directivities with those calculated on

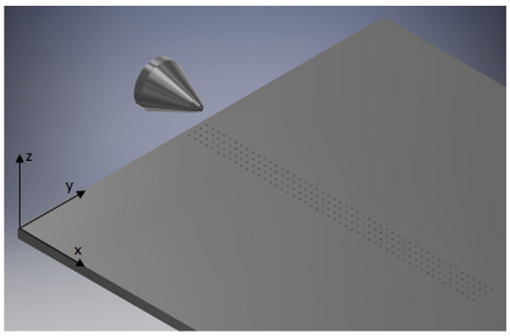

(a) Sketch of the experimental setup.

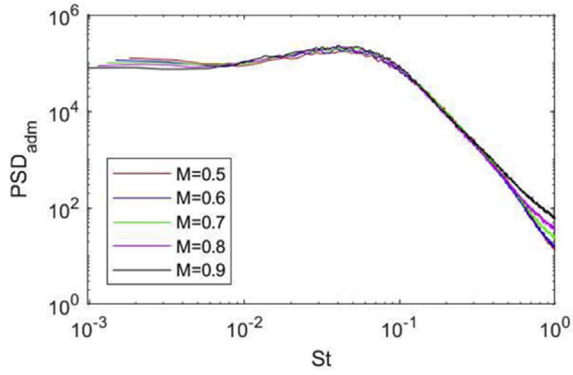

(b) PSD_{adm} at $x/D = 15$.

Fig. 17.

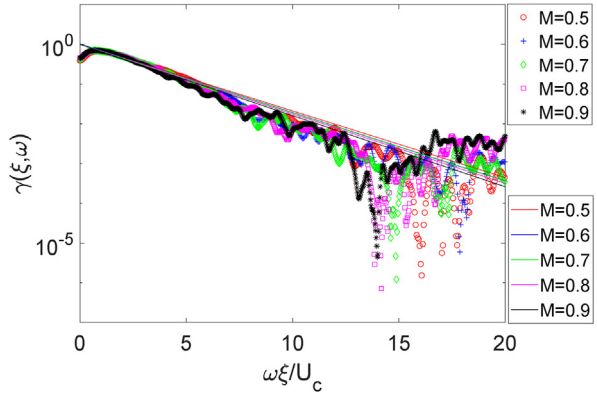

Fig. 18. Wall pressure coherence at $x/D = 25$ (markers) and Corcos' fit (line).

basis of the aforementioned analytical model has demonstrated good correspondence between the two. Further development of the experimental techniques for the installed jet (e.g., in presence of coflow) can be quite valuable.

Written by Victor Kopiev: vkopiev@mktsagi.ru, *TsAGI, Russia.*

4. Helicopter noise

4.1. DLR experimental and numerical methods for the study of helicopter acoustic scattering

The scattering of noise generated by helicopter rotors has been recognized as having a significant influence on both the noise spectra and the noise directivity. To date, there has not been an extensive research effort towards the comprehension of the phenomenon. This is particularly important when dealing with the tail rotor noise, for which the wavelength of the

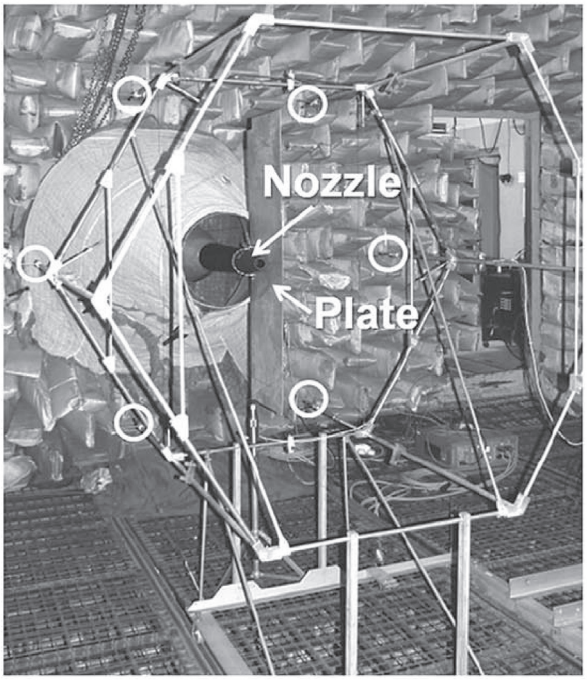

Fig. 19. Representation of experimental setup (microphones positions are highlighted by the circles).

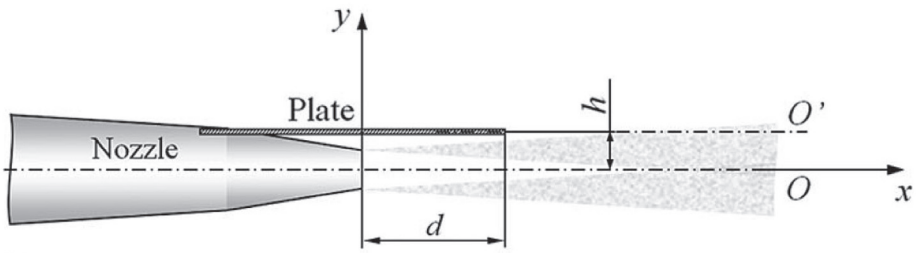

Fig. 20. Side-view sketch of the jet–plate system.

harmonics is comparable or smaller than the characteristic dimension of the fuselage. To boost research activities on the topic of noise propagation in the presence of the fuselage a specific Action Group (AG) 24 [29,30] has been instituted in the Group for Aeronautical Research and Technology in EURope (GARTEUR). The GARTEUR AG24 shielding experiments were conducted in DLR's Acoustic Wind tunnel in Braunschweig (AWB), where the scattering for generic configurations was studied using two point sources and one rotor source. Fig. 21 demonstrates the generic acoustic shielding experiment. First a sphere has been used as a shielding object then, a GARTEUR helicopter model has been investigated (Fig. 21). The GARTEUR helicopter model consists of an ellipsoid fuselage, cylindric tail boom and a simple empennage. Comparisons of the experimental results, obtained using the laser sound source methodology [31], with the numerical simulations have been carried out. The numerical results are obtained using DLR's fast multipole boundary element method (FMCAS) code [32,33] which solves the exterior Helmholtz problem for the scattered pressure field. Fig. 22a shows the contour plot of the shielding factor from numerical simulations on a receiving plane (microphones) for the GARTEUR Helicopter model. The general shielding characteristics can be observed by the higher and lower levels represented by different colors and a cancellation of the sound waves is observed. The comparisons with the experimental results taken by a microphone array along the center line are given in Fig. 22b. The comparison shows a very good agreement in terms of amplitude and phase. In the framework of AG24, a unique noise scattering database was established through dedicated wind tunnel tests, enabling the assessment, and further development, of current noise scattering prediction tools capabilities.

Written by Jianping Yin: jianping.yin@dlr.de, *Karl-Stéphane Rossignol, DLR Germany*.

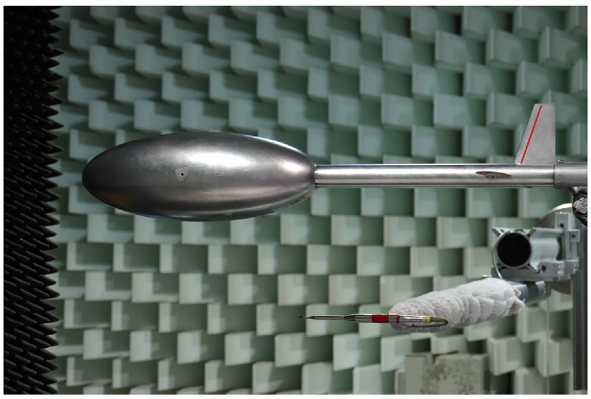

Fig. 21. Test set-up of the GARTEUR Helicopter model for the acoustic shielding tests in AWB using the laser sound source methodology.

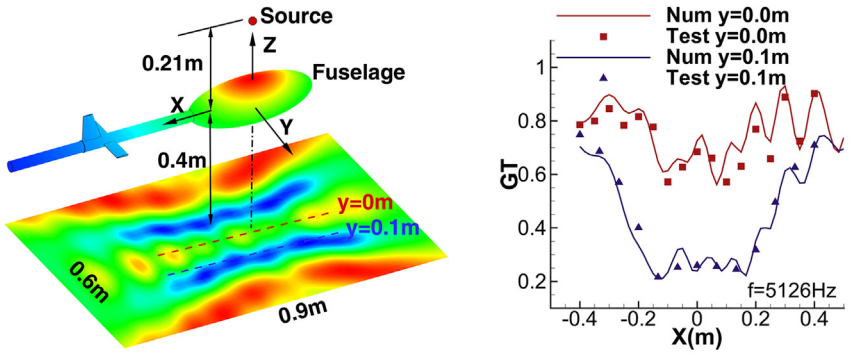

(a) Simulation.

(b) Comparison of noise shielding factor with simulation at y=0m and y=0.1m

Fig. 22. Noise scattering by GARTEUR helicopter model.

5. Aircraft interior noise

5.1. Flow-induced vibrations and noise simulation using unit-cells finite element models

The flow-induced vibrations and noise levels must be predicted before operating aircraft systems. However, the vibroacoustic analysis of structures under distributed stochastic excitation is often limited due to high computational costs, especially in the medium frequencies. Within the framework of flat and/or curved homogeneous and periodic structures, a unit-cell approach is developed in order to overcome the state of the art in terms of computational speed, maintaining, at least, the same accuracy of the standard FE-based techniques. First, a 1D WFE (Wave Finite Element) scheme is developed to deal with random excitation of flat, curved and tapered finite structures: multi-layered and homogenised models are used [34]. In this case a single substructure is modelled using finite elements. At each frequency step, one-dimensional periodic links among nodes are applied to get the set of waves propagating along the periodicity direction and the method can be applied even for cyclic periodic systems. The set of waves is successively used to calculate the Green transfer functions between a set of target degrees of freedom and a subset representing the wetted (loaded) ones. Subsequently, using a transfer matrix approach, the flow-induced vibrations are calculated in a FE framework [34]. A 2D WFE approach is developed in combination with a wavenumber-space load synthesis to simulate the sound transmission of infinite flat, curved and axisymmetric structures [35]: both homogenised and complex periodic models are analysed, as in Fig. 23. In this case, finite-size effects are accounted for using a baffled window equivalence for flat structures and a cylindrical analogy for curved panels. The presented numerical approaches have been validated through analytical, numerical and experimental results for different test cases and under different random load conditions. In particular, analytical response and classic FEM have been used as references to validate the flow-induced vibrations of plates and cylinders under a turbulent boundary layer load. From the experimental point of view, the approach has been validated comparing results in terms of transmission loss evaluated on real aircraft fuselage panels (composite honeycomb and ribbed curved panels, as in Fig. 23.) under diffuse acoustic field excitation [36]. **EU Project** Sponsor**: VIPER (H2020 MSCA G.A. 675441) - Mohamed Ichchou, Ecole Centrale de Lyon**.

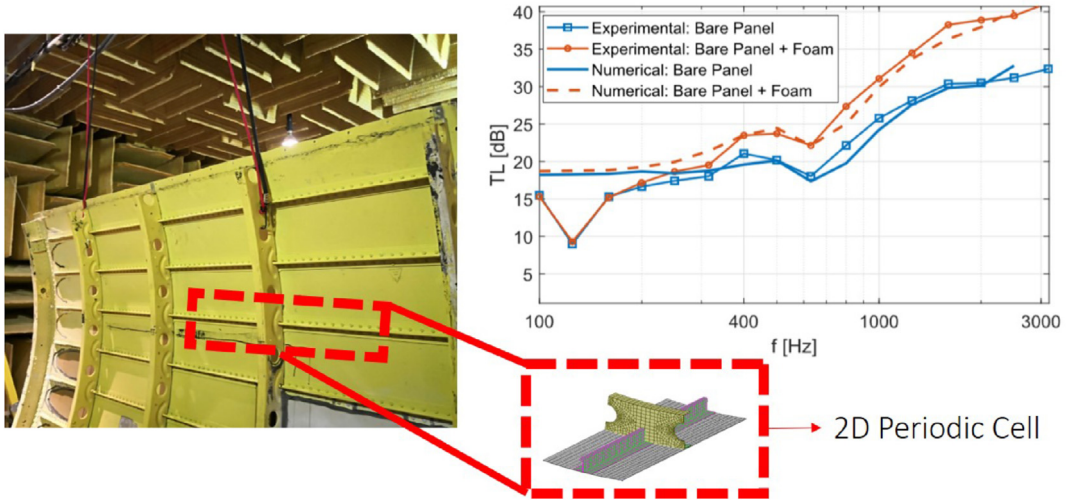

Fig. 23. Sound Transmission Loss of a curved fuselage panel under diffuse acoustic load, in bare configuration and with attached porous layers. A 2D WFE approach is used for the numerical simulations.

(a) SEA model of a fuselage section.

(b) OASPL over the cavities present in the fuselage section.

Fig. 24.

Written by F. Errico: fabrizio.errico@ec-lyon.fr, *S. De Rosa, Università di Napoli Federico II, Italy, F. Franco, Università di Napoli Federico II, Italy, M. Ichchou, Ecole Centrale de Lyon, France.*

5.2. Aicraft interior noise evaluation by Statistical Energy Analysis method

Vibro-acoustic analysis is a necessary step for the virtual design of aerospace structures. In order to reduce the design costs and to maximize the acoustic performance of aerospace structures, a robust and mature prediction of interior noise levels is required. Interior noise is an essential topic to be considered in the design and operation of all aerospace flight vehicles. Noise is due to the combination of different sources such as: powerful propulsion systems, high-speed aerodynamic flow over vehicle surfaces and operation of on-board systems (air conditioners, pressurization system). The evaluation of the Sound Pressure level, for the medium-high frequency range, of an aircraft fuselage section (Fig. 24a) at different stations and locations inside the cabin has been performed numerically [37] by using Statistical Energy Analysis (SEA) method. Different configurations have been considered for the analysis: from the benchmark empty cabin: only primary structure - conf. A, up to the "fully furnished" one: primary structure with interiors and noise control treatments - conf. E. These results, reported in Fig. 24b, are essential to understand which are the main parameters affecting the noise insulation. Furthermore, the Power Inputs evaluation has been determined to determine the contribution of each considered aeronautic component on the acoustic insulation. Finally, the effect of a viscoelastic damping layer embedded in the glass window has been evaluated.

Moreover, in order to improve the comfort, and hence to reduce the Sound Pressure Level in the cabin, different fuselage configurations, in terms of materials used for lining panels, are compared. To this aim, two types of analysis have been performed: the first one at material level and the second one at system level. At material level, a new acoustic metamaterial (Fig. 25a), consisting of a poro-elastic melamine matrix with cylindrical aluminium inclusions, has been proposed to reduce the noise in the cabin. In order to analyse the metamaterial by using commercial softwares, a novel homogenization method based on CUF and MSG has been successfully extended to the computation of effective properties of these materials. In particular, an investigation has been carried out in Actran to verify if this homogenization model captures the acoustic properties (in terms of Transmission

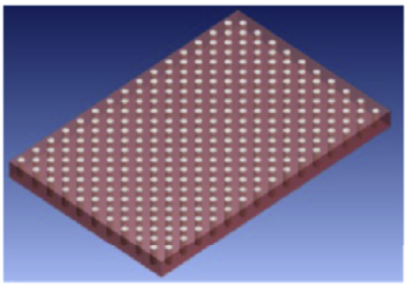

(a) Metamaterial.

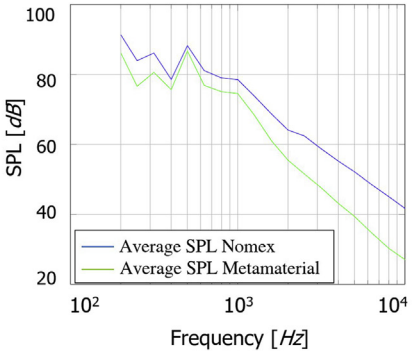

(b) Comparison of the average Sound Pressure Level (SPL) for all the head acoustic cavities of the fuselage for two different core materials.

Fig. 25.

Loss) of the metamaterial. The results obtained by studying the metamaterial as heterogeneous and homogeneous have shown an average good agreement along the frequencies. At system level, the metamaterial has been used as core of the sandwich lining panel of a regional turboprop fuselage and its promising performances have been investigated by using SEA analysis available in VA One. In particular, two configurations of fuselage have been considered: one with lining panel with Nomex core (baseline) and the other one with lining panel with metamaterial core. The SPL at the head of the passenger and the overall sound pressure level in the cabin have been measured and it has been demonstrated that the configuration with metamaterial core behaves better than Nomex in the overall frequency range (Fig. 25b).

Written by PETRONE Giuseppe: giuseppe.petrone@unina.it, *Department of Industrial Engineering, Aerospace Division, University of Naples Federico II, Naples, Italy and CINEFRA Maria, Department of Mechanical and Aerospace Engineering, Politecnico di Torino, Turin, Italy*.

5.3. Simulation of Airbus-A320 fuselage surface pressure fluctuations at cruise conditions

The fuselage surface pressure fluctuations on an Airbus-A320 aircraft at cruise conditions are simulated by solving a Poisson equation [38]. The right-hand-side source terms of the Poisson equation, including both the mean-shear term and the turbulence-turbulence term, are realized with synthetic anisotropic turbulence generated by the Fast Random Particle-Mesh Method [39]. The stochastic realization is based on time-averaged turbulence statistics derived from a RANS simulation under the same condition as in the flight tests, conducted with DLR's Airbus-A320 research aircraft. The fuselage surface pressure fluctuations are calculated at three streamwise positions from front to rear corresponding to the measurement positions in the flight tests [40,41]. One- and two-point spectral features of the pressure fluctuations relevant to the fuselage surface excitation are obtained and analysed.

The simulated one-point spectra show good agreement with the measured results for all three calculation positions up to 5 kHz, which is the upper frequency range of interest in the industrial application, see Fig. 26. The rapid roll-off at high frequencies for the mid and aft positions is mainly related to the numerical mesh resolution, which cannot resolve the fine structure of the turbulence close to the surface. Fig. 27 shows the obtained wavenumber-frequency spectrum at the front position, which is in good agreement with the measured spectrum. Due to the small misalignment between the flow direction and the fuselage longitudinal axis at the front position, both simulated and measured spectra show a slight inclination against the k_3 axis. Through the peak position of the wavenumber-frequency spectra, the convection velocity can be calculated. The obtained velocities for all three positions are consistent with that obtained from the measured results, see Fig. 28.

Written by N. Hu: nan.hu@dlr.de, *C. Appel, S. Haxter, DLR, Germany, S. Callsen, A. Klabes, Airbus Operations GmbH, Germany*.

6. Propeller noise

6.1. Noise reduction of counter rotating propellers through a locked blade row

We reported an invention concerning counter rotating open propellers (CROR) for applications in general aviation, and possibly for smaller electrically powered vehicles [42]. We propose locking one blade row at take-off/climb-out and final descent of a fixed-wing aircraft the locked blade row is re-engaged at cruise, where higher efficiency is very important. By using a reduced-

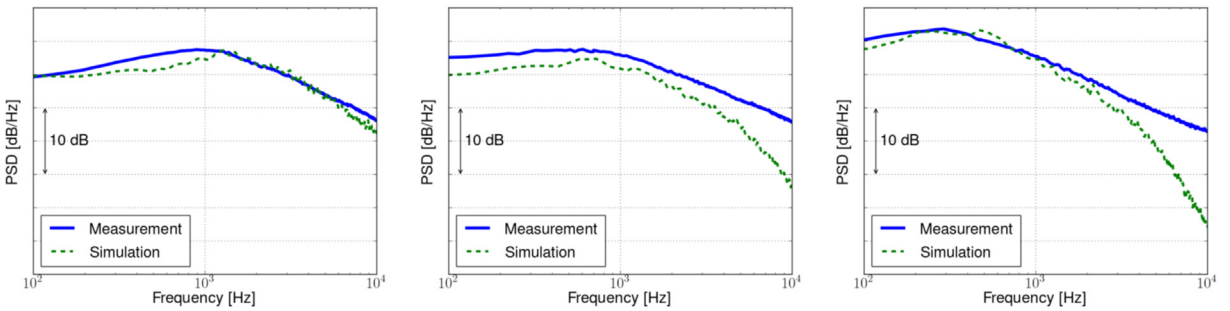

Fig. 26. One-point spectra at different streamwise positions, (left) front (middle) mid (right) aft.

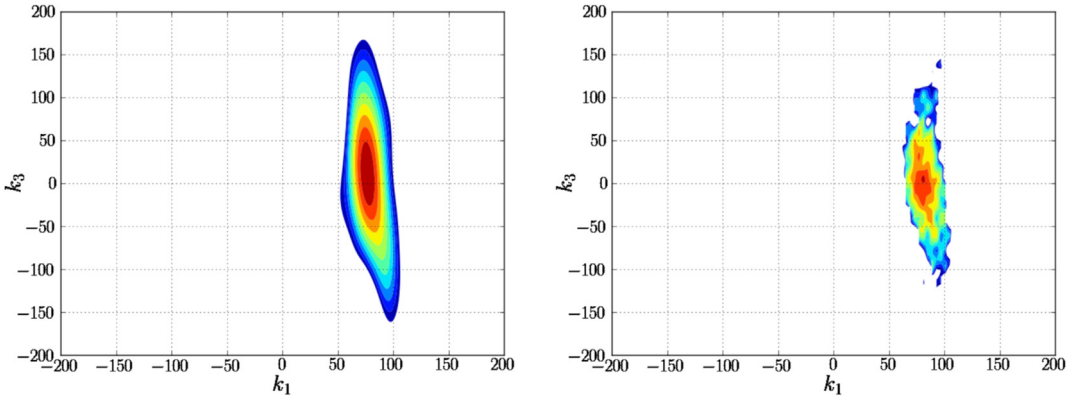

Fig. 27. Contour plots of wavenumber-frequency spectra at 2417 Hz for the front position, levels between −10 dB and 0 dB with increment of 1 dB, (left) simulation (right) measurement.

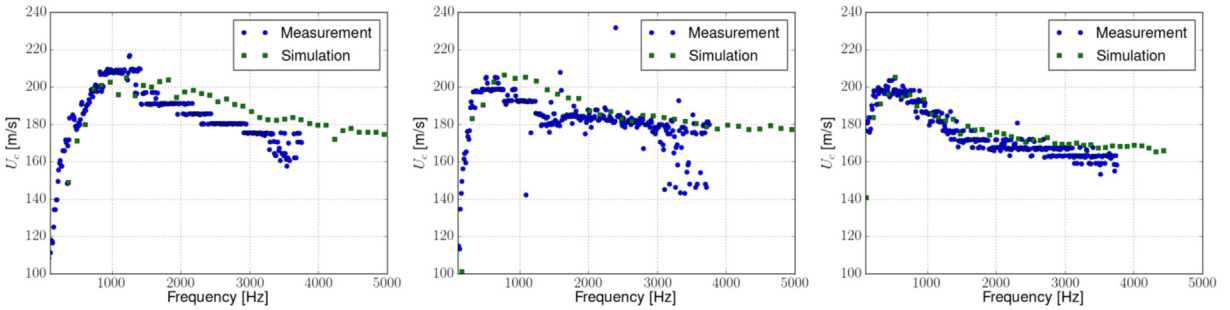

Fig. 28. Convection velocities at different streamwise positions, (left) front (middle) mid (right) aft.

order acoustic model coupled to an aerodynamic model, we demonstrate that for a number of configurations and blade counts it is possible to greatly reduce noise. For example, with a locked-fore and locked-aft configuration resulted in a maximum noise reduction of around 3 dBA (3 EPNLdB) and 3 dBA (6 EPNLdB), respectively. We further investigate novel configurations, such as variable-diameter fore rotor (with locked-aft rotor) and foldable aft rotor. Increasing the fore-rotor diameter by 30% was shown to reduce noise by up to 8 dBA against an operative CROR of the same tip extension. Folding of the aft rotor backward produces a maximum noise gain of 12 dBA. These gains are achieved against a loss of efficiency of a few percent, in comparison with the optimal condition when the blade rows are both rotating. This slight loss of efficiency is time-limited, as most of the CROR would operate as by design. The constraints include the delivery of the required thrust or power (trim condition). CROR design must be carried out in such a way that the propulsive system is capable of operating as a single rotor in the most critical conditions, and research is underway to carry out various optimisations and off-design analysis. The technical literature contains several concepts to reduce noise from CROR, but our contribution explores a completely new configuration that is aimed at low to medium power outputs.

Written by Antonio Filippone, a.filippone@manchester.ac.uk, *The University of Manchester, United Kingdom.*

7. Techniques and methods in aeroacoustics

7.1. Effect of turbulent boundary layer induced coherence loss on beamforming measurements in industrial scale wind tunnel tests

Testing the noise reduction technologies and innovative aircraft geometry modifications is key in developing of the silent aircraft of the future. For this reason, scaled models are used to perform aeroacoustic wind tunnel tests. To assure that the test is representative, i.e., high model fidelity, for the full scale flight the model is currently still considerable large (5–8 m span). This requires the operation of large wind tunnel facilities such as the Large Low-speed Facility (LLF) of the German-Dutch Wind Tunnels (DNW). This wind tunnel can be operated in closed and open test section configuration. The interaction of the sound produced by the aircraft and the turbulent shear layer in the open configuration can lead to severe coherence loss which reduces the quality of the measurement, consequently, the ability to design improvements and predict full scale noise production, etc.. To avoid this issue a closed test section can be used. However, in the closed test section, the large scale of the wind tunnel still leads to boundary layers of approximately 20 cm thick. This raises the question if turbulence induced coherence loss might still influence results.

Modelling the coherence loss in cross-spectral matrix estimations and subsequently performing conventional beamforming showed that the expected loss of source power is neglectable up to frequencies of 10 kHz. Frequencies from 20 kHz could potentially lose 1-3 Decibels in source power up to 4-6 Decibels at a frequency of 50 kHz [43]. These numbers where calculated using a measurement from a model as input to assure a relevant test case. A key input for the model is the two-dimensional structure function, constituted by the statistics of the turbulent structures of the flow. Good predictions and or measurements of the structure function will be further investigated.

Written by Leandro de Santana: leandro.desantana@utwente.nl, *University of Twente, The Netherlands*.

7.2. Perception-based evaluation of auralized future low-noise aircraft concepts

To effectively reduce aircraft noise and its impacts on residents around airports, developments of low-noise strategies should consider the perception of sound [44]. To that aim, in Refs. [45] a comprehensive simulation approach is presented for the assessment and optimization of novel aircraft designs and flight procedures regarding perceived sound. The paper proves its feasibility by an application study on narrow-body twin-engine jet airliners. In this study, the effects of airframe modifications (e.g. landing gear mesh fairing, slat droop nose design, FOPP vortex generators), novel aircraft design, and tailored flight procedures on perceived annoyance are investigated. The key ingredient of the approach is the use of auralization for listening experiences of currently non-existing air vehicle flyovers in a virtual acoustic environment. First, aircraft and flight trajectories are designed [46]. Second, spectral sound emission of each partial source along the flight trajectory is predicted using parametric models. Third, emission sounds are synthesized and propagated to ground-based observer locations with time-varying digital filters that simulate propagation effects such as Doppler effect, atmospheric absorption and turbulence-induced amplitude modulation (Fig. 29). Multiple observer locations along the flight path are simulated to represent different exposure situations with varying noise source mixtures. The observer signals are spatialized for a hemi-spherical loudspeaker array. This allows listeners to experience the design parameters under varying operational conditions. With a psychoacoustic laboratory experiment, the changes in short-term noise annoyance to different low-noise technologies are measured (Fig. 30). Significant annoyance reductions were found for the studied design parameters. Maximum benefit was achieved by the combined modification of the air vehicle and the flight procedure.

Written by: Reto Pieren: reto.pieren@empa.ch, *Empa, Switzerland, Lothar Bertsch, DLR, Germany, Beat Schäffer, Empa, Switzerland*.

7.3. Pressure-field permeable-surface integral formulations for sound scattered by moving bodies

Two novel integral formulations for the prediction of sound scattered by moving bodies are introduced in Refs. [47]. Derived from the Lighthill and the Ffowcs Williams and Hawkings equations for the pressure field, they are expressed in the frequency-domain over a permeable (fictitious) surface surrounding the scatterer(s), and are numerically evaluated through application of a boundary element technique. The work presented in Refs. [47] deals with the assessment of the influence of the nonlinear terms of Lighthill and Ffowcs Williams and Hawkings equations on sound scattering prediction in the presence of nonuniform mean-flow due to scatterer motion, the assessment of the corresponding limits of applicability of the widely-used linear formulations for solid-wall boundaries, and the development of integral formulations capable to predict accurately and efficiently the noise scattered in the far field by moving bodies. In addition, it provides the results of a numerical investigation concerning a non-lifting wing in uniform translation impinged by an acoustic disturbance generated by a co-moving source, and including the comparison of the results obtained through the proposed scattering formulations with those given by a boundary-field velocity-potential approach recently validated for moving-body problems [48]. The main outcomes of Ref. [47] reveal that, when the proposed pressure-field formulations include the nonlinear terms through application of a suitable permeable-surface, their predictions match those provided by the boundary-field velocity-potential solver, whereas the fully linear versions of both pressure-field approaches yield underestimated scattered noise predictions, significantly less accurate than those given by the

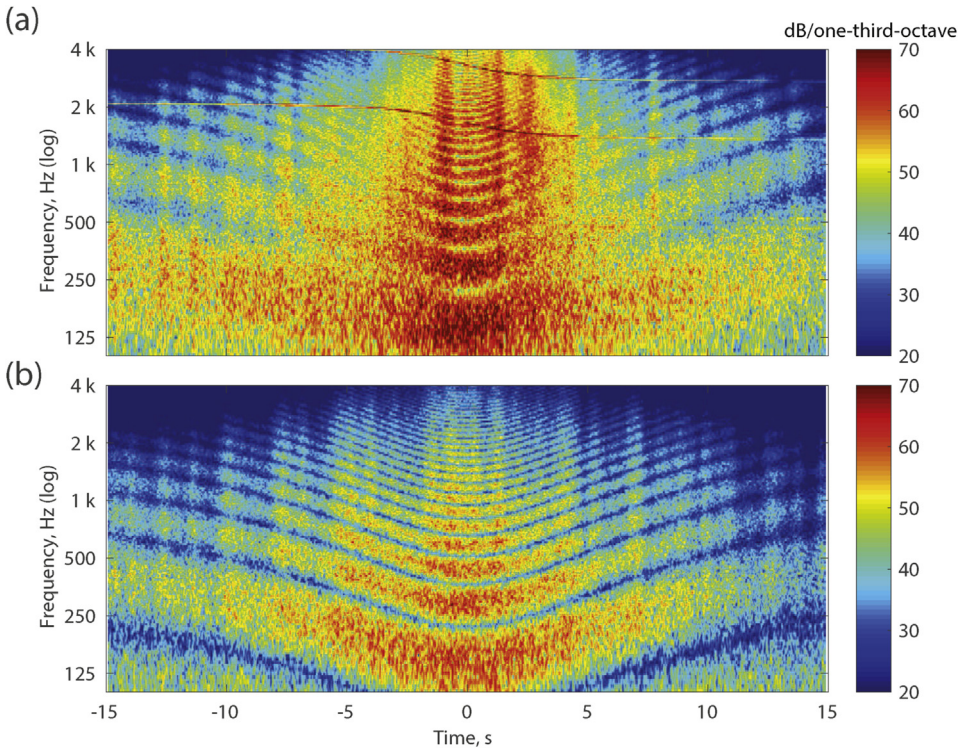

Fig. 29. Spectrograms of synthesized flyover sound pressure signals for a reference aircraft (A319-100) on a standard approach procedure (a) and a novel aircraft design on its tailored approach procedure (b) as received 1.2 m above ground at 4 km to touch-down.

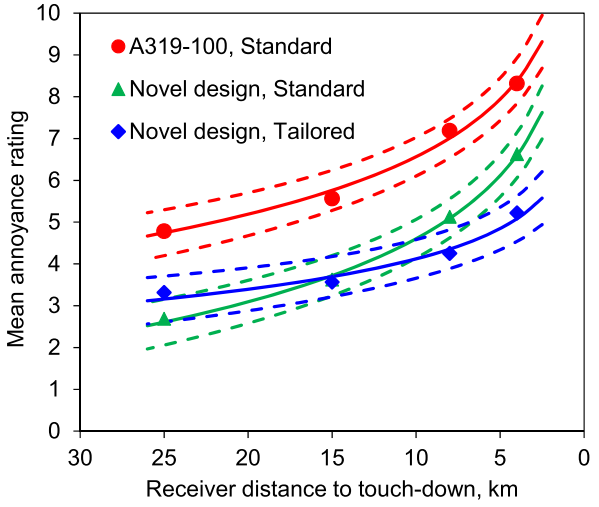

Fig. 30. Mean measured noise annoyance of an existing reference aircraft and a novel vehicle design on a standard and tailored approach as a function of the receiver location. Symbols show measured data. Lines show statistically modelled data including confidence bands.

linear version of the velocity-potential formulation.

Written by Massimo Gennaretti: massimo.gennaretti@uniroma3.it, *Department of Engineering, Roma Tre University, Italy*.

7.4. Post-processing for direct aeroacoustic simulations using Helmholtz's decomposition

The well-known Helmholtz decomposition for vector fields has been reformulated for finite-dimensional domains. Thereby, the compressible velocity field (see Fig. 31) is decomposed into vortical and compressible structures (see Fig. 32) and the arising

partial differential equations have been solved by the finite element method [49,50]. Modifications to the ordinary Helmholtz decomposition and its application have been studied [51]. In particular, two different formulations were compared. The derived formulations ensure orthogonality considering appropriate boundary conditions. Concerning non-convex domains, we found out that the vector-potential formulation behaves superior. The capabilities of Helmholtz decomposition as a post-processing tool for direct simulation of flow and acoustics are demonstrated by theoretical and practical considerations. The scalar-potential formulation is computationally efficient but applies to convex domains only. Thus, we motivate the use of the curl-curl equation (vector-potential formulation), since it is accurate at acoustically relevant regions such as re-entrant corners. The proposed vector-potential formulation is suitable for transonic flows, an arbitrary control volume, and separates typical eddy structures accurately from compressible effects. The application of the developed decomposition to a compressible flow field over a rectangular cavity at Mach 0.8 shows promising results (see Fig. 32) for further applications and the development of acoustic boundaries in fluid dynamics. To conclude, the given formulations are a powerful post-processing tool for direct aeroacoustic simulations.

Written by Stefan Schoder: stefan.schoder@tuwien.ac.at, *Manfred Kaltenbacher:* manfred.kaltenbacher@tuwien.ac.at.

7.5. Numerical assessment of open-rotor noise shielding with a coupled approach

Contra-Rotating Open Rotors promise substantial propulsive efficiency improvements compared to conventional jet engines, albeit at significantly increased sound emissions. In addition to constructive measures like rear rotor radial clipping, the shielding effects of engine integration into the aircraft empennage may help to mitigate unacceptable noise levels and are therefore of special interest to research efforts in this area.

In contrast to earlier investigations on shielding and reflection of noise on helicopters [52], which considered these effects by a large integration surface in the Ffowcs Williams-Hawkings evaluation surrounding the complete rotorcraft, the current approach separates noise emission and further scattering phenomena in a coupled approach [53]. Sources are handled again by high-fidelity CFD in the vicinity of an isolated CROR [54], and the incident sound field is afterwards evaluated on the scattering surface, in this case the airframe of a generic jet empennage. Further shielding, diffraction and reflection effects are handled by our fast multi-pole BEM tool ScatMan solving the Helmholtz equation. As this requires the acoustic particle velocity in addition

(a) ρ/ρ_0 (b) $\| \boldsymbol{u}/U_\infty \|$

Fig. 31. Plots of the flow results and the decomposition of the Mach 0.8 cavity. (a) The relative density of the flow field displays compressible flow structures and the resulting acoustic wave propagation in the flow domain. (b) The magnitude of the flow velocity indicates the presence of the shear layer mode.

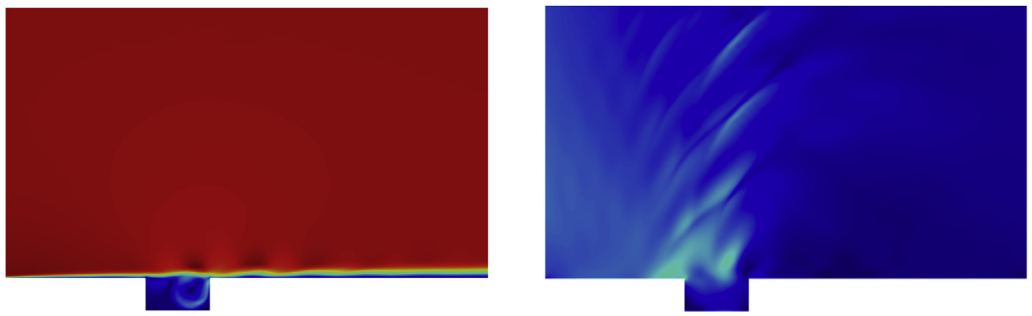

(a) $\| \boldsymbol{u}^{\mathrm{v}}/U_\infty \|$ (b) $\| \boldsymbol{u}^{\mathrm{c}}/U_\infty \|$ in 10^{-1}

Fig. 32. Plots of the decomposition of the Mach 0.8 cavity. (a) Vortical velocity component of the Helmholtz decomposition. (b) Compressible velocity component of the Helmholtz decomposition.

to the incident sound pressure on the evaluation surface, the FW-H approach of our ACCO tool was extended by the Möhring analogy, enabling the consideration of a uniform background flow field [55]. Both ACCO and ScatMan are integrated into the advanced rotorcraft simulation framework developed at IAG.

The separation of expensive high-fidelity CFD on the isolated CROR and subsequent acoustic integration on the airframe allows the cost-efficient evalution and assessment of several variants, for example different empennage layouts (see Figs. 33 and 34). A further parameter study reveals the potential of longitudinal engine position optimization (Fig. 35).

Written by Manuel Keßler: kessler@iag.uni-stuttgart.de, *Lukas Dürrwächter, Ewald Krämer, Institute of Aerodynamics and Gas Dynamics, University of Stuttgart, Germany*.

7.6. A hybrid zonal prediction method for noise from a porous trailing-edge

Carefully placed porous materials offer the possibility for airframe noise reduction. Airframe noise arises from the interaction between an airframe geometry and a turbulent flow, e.g., the noise generated by a wing's trailing edge [56]. The scale-resolving simulation of noise reduction by porous material is challenging due to the high Reynolds number and the associated large scale-disparity between the small pore sizes and the large (hydrodynamic) scales. In this contribution, we present a novel Overset-LES method capable of resolving the turbulent sound sources where the porous material is modelled by a volume-average approach [57].

As the turbulence swipes over the trailing edge, it does not significantly penetrate the porous material. Therefore, a volume-average modelling is justified, leading to a Darcy (linear friction) and Forchheimer terms in the momentum equations, while still allowing to simulate high Reynold-number flows. In Fig. 36, a numerical Schlieren image illustrates the qualitative differences between the solid and porous trailing-edges, i.e., small scale dynamics above the surface of the porous insert. This

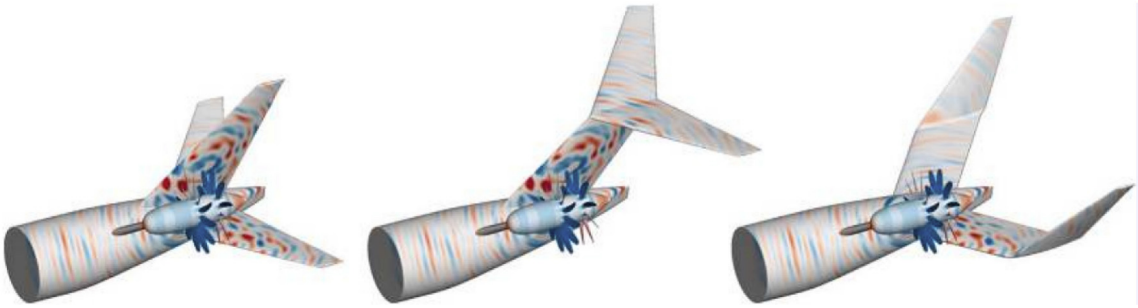

Fig. 33. Instantaneous incident sound pressure.

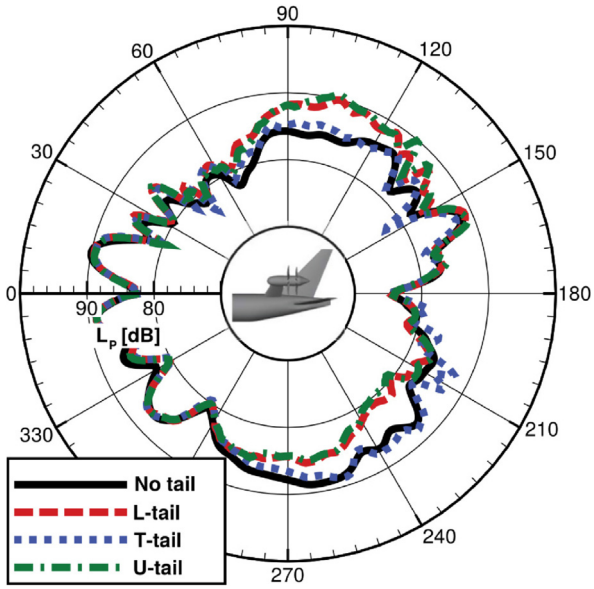

Fig. 34. Polar directivity of different tail configurations.

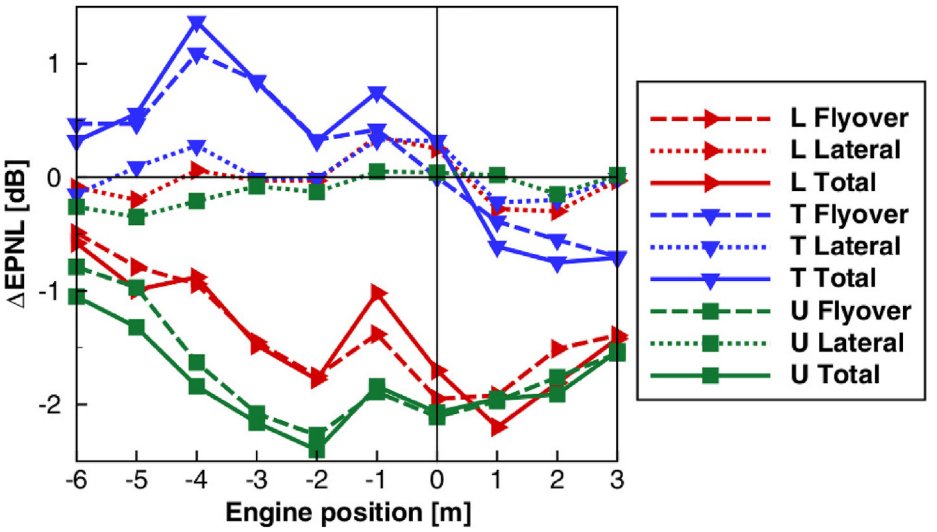

Fig. 35. EPNL changes due to longitudinal engine shift.

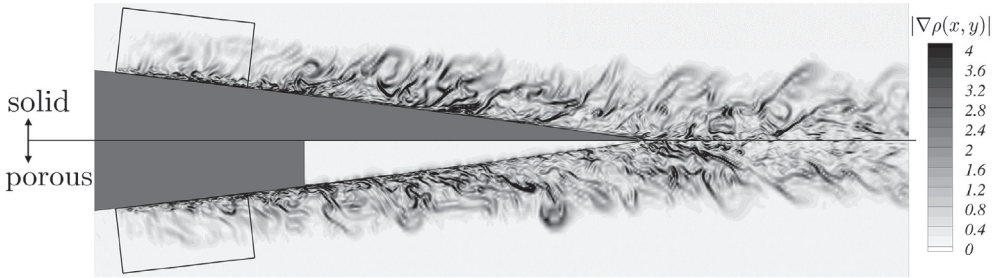

Fig. 36. Magnitude of density gradients by instantaneous Schlieren-like view (in arbitrary unit) of a vertical plane, comparing solid trailing-edge (upper part of the plot) and porous inset at trailing edge (lower part). Rectangular box represents the upstream region of the Overset-LES domain with inflow forcing.

increased high-frequency noise is due to the porous surface roughness, which is indirectly accounted for by the boundary condition between porous-fluid interface. The surface-pressure spectrum at the trailing edge, see Fig. 37a, confirms the numerical Schlieren image: increased surface-pressure amplitudes at high frequencies. However, this does not subsequently lead to a noise increase in the far-field SPL (see Ref. [57] for a discussion). Fig. 37b rather shows a reduction of 2–4 dB. The porous simulations agree well with experimental measurements (from Ref. [58,59]) for the both solid and porous cases and provide insight into the

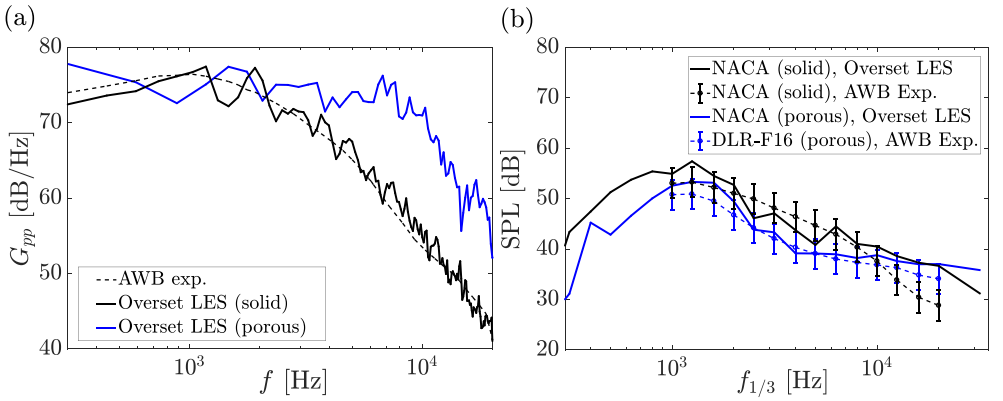

Fig. 37. (a) Surface-pressure spectrum G_{pp} at trailing edge ($x/c = 0.99$ for the solid and porous case). (b) Far-field pressure spectrum at 1 m distance above the trailing edge. Experiments from Ref. [58,59].

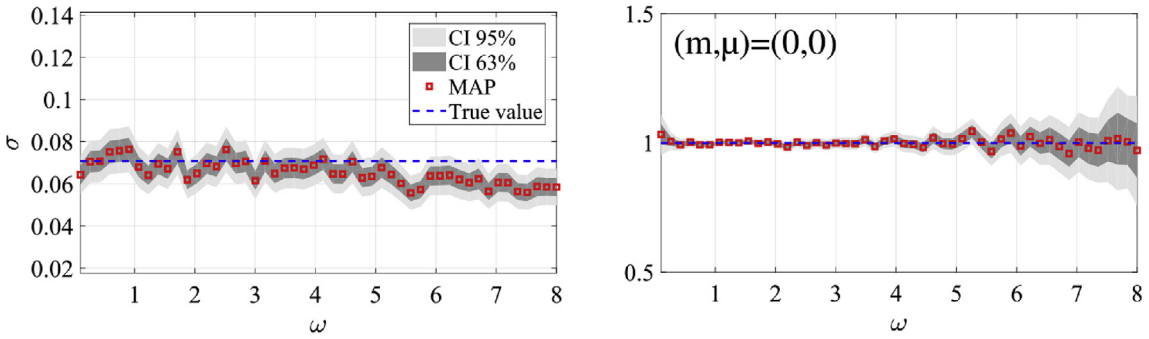

Fig. 38. Inference results in the no flow case. Identification of the noise level σ and the plan wave mode, as a function of the normalized frequency ω.

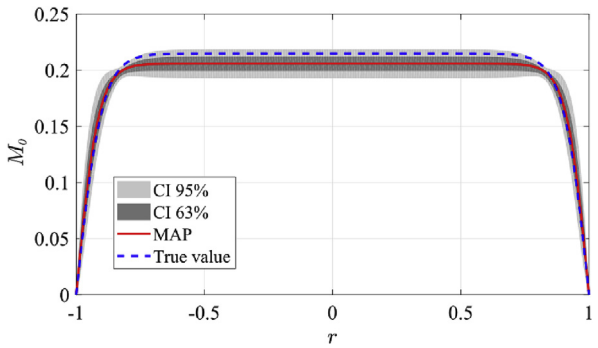

Fig. 39. Comparison between inferred flow profile and true profile at $\omega = 5$. MAP: Maximum A Posteriori, CI: Credibility Intervals.

noise reduction mechanisms by porous materials [57].

Written by P. Bernicke: p.bernicke@tu-braunschweig.de, *R.A.D. Akkermans, V.B. Ananthan, TU Braunschweig, Germany, R. Ewert, J. Dierke, L. Rossian, DLR, Germany.*

8. Miscellaneous topics

8.1. Bayesian inference for modal identification in ducts with a shear flow

The characterization of the modal structure of the noise that propagates within a duct in the presence of a shear grazing flow is a pre-requisite to the study of acoustic liner efficiency in representative configurations, where many modes are present (i.e., engine nacelle inlet and exhaust, environmental control systems). In its effort towards the reduction of aircraft noise, ONERA has developed a statistical inference modal decomposition of in-duct pressure fields that allows for uncertainty considerations [60]. Coupling pressure wall measurements to the solution of the 1D linearized Euler equations and a Bayesian inference strategy allowed the correct modal identification in the presence of a general shear grazing flow (Fig. 38). It was simultaneously shown possible to infer the flow profile parameters using the same measurements (Fig. 39). This is due to the separate acoustic modes reacting differently to the presence of a shear grazing flow, thus allowing for identification of its parameters if enough observations of the acoustic field are made. High-order modes were shown to be easier to identify at high frequency, which might initially seem counter-intuitive to the experimentalist. This phenomenon was explained by an increased correlation between low-order modes caused by the localization of their wavenumbers as the frequency increases.

Written by Rémi Roncen: remi.roncen@onera.fr, *F. Méry, ONERA, France, E. Piot, ONERA, France.*

8.2. Direct noise computation for automotive cabin noise predictions

Noise prediction is becoming increasingly important for the automotive industry due to increasing comfort demands of customers. As engine and tire noise has continuously decreased, aerodynamic noise has become increasingly important. Aerodynamic noise is even dominant for vehicle speeds exceeding 80 km/h and mainly results from the exterior side-mirror and the A-pillar. Although the acoustic pressure fluctuations are orders of magnitude smaller than the turbulent fluctuations, the generated sound (above 800 Hz) is more efficient in exciting side window vibrations (thereby transferring the acoustics to the interior cabin). In this contribution, a finite volume method is utilized for the direct noise computation (DNC) of a generic vehicle model

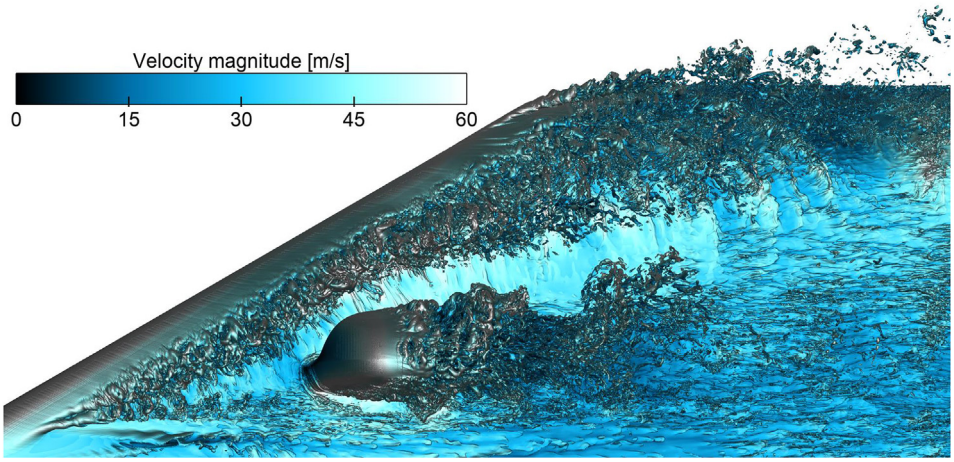

Fig. 40. Iso-surfaces of the vorticity field (5000 1/s) in the region of the A-pillar, exterior mirror and side window.

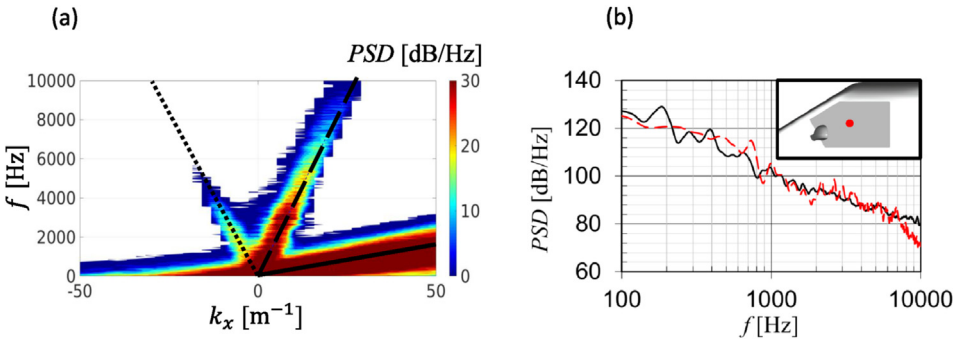

Fig. 41. (a) Frequency-wavenumber spectrum (at $k_z = 0$) of SAE body with side mirror. The black solid represents the convective branch, dashed one the acoustic branch (wave propagating in positive x-direction), and dotted one the spurious noise branch. (b) PSD spectra of the side window's normal acceleration. Solid line represents wind tunnel measurement and dashed line vibro-acoustic result based on DNC. Inset shows accelerometer position used for the comparison.

(a modified version of the SAE-body) with a real side mirror and A-pillar [61].

In Fig. 40 the flow field is illustrated by iso-vorticity contours, showing the separated A-pillar vortex and the side-mirror's wake. Fig. 41a shows the frequency-wavenumber spectrum at $k_z = 0$, where three branches can be observed: a convective hydrodynamic branch (solid line), a positive acoustic branch (dashed) of waves propagating in the positive x-direction, and a spurious noise branch (dotted) of spurious waves propagating in negative x-direction. The positive acoustic branch was shown to be related to the side mirror by a careful analysis of simulations without a side mirror. The upstream traveling waves originate from downstream mesh refinement interfaces and are therefore spurious noise (which are selectively damped, see Ref. [62,63]). Fig. 41b shows a good agreement between the numerically and experimentally obtained vibro-acoustic spectra. Deviations at low- and high-frequency are due to short signal time and mesh resolution, respectively. It illustrates the applicability of DNC for cabin noise studies in the automotive branch [61].

Written by Ali H. Dawi: ali.dawi@volkswagen.de, *Volkswagen AG, Germany, R.A.D.Akkermans, TU Braunschweig, Germany*.

8.3. Influence of turbulent oncoming flow and vehicle-excited turbulence on the wind noise inside a vehicle

The aeroacoustic development of vehicles is, for reasons of reproducibility, mainly done in wind tunnels under steady flow conditions with low turbulence level. In a real situation on road, however, a vehicle experiences unsteady, turbulent flow. The flow variations lead i. a. to modulations of the wind noise inside the cabin, which affect the passenger's quality impression. This unsteadiness has to be taken into account in the vehicle development process. Therefore, methods for the realistic and reproducible determination of unsteady wind noise have been developed. These include active turbulence generation systems in wind tunnels as well as quasi-steady simulation methods [64]. To analyse the unsteady wind noise in detail, a methodology to subdivide the modulations according to their origin based on quasi-steady simulation methods has been derived [65]. The modulations are divided into those generated by turbulent oncoming flow and those generated by vehicle-excited turbulence. The latter is excited by the geometry of the vehicle, even in steady flow. The methodology has been applied to analyse the mod-

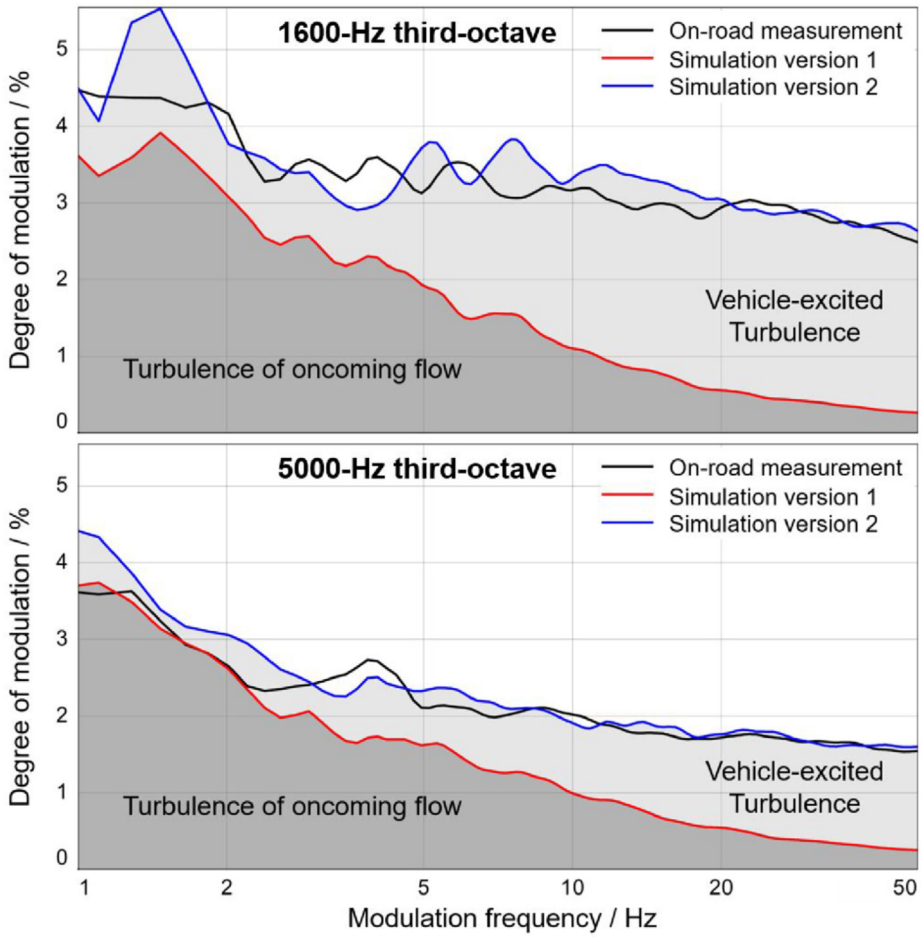

Fig. 42. Modulation spectra of the 1600-Hz and 5000-Hz third octave bands. Separation of modulations from turbulent oncoming flow (dark grey area) and those from vehicle-excited turbulence (light grey area).

ulations for a given vehicle and an exemplary unsteady oncoming flow. Fig. 42 shows the results for the 1600-Hz and 5000-Hz third-octaves. For all considered third-octave bands from 800 Hz to 8000 Hz, the influence of the oncoming flow turbulence is comparable. With decreasing third-octave centre frequency, however, an increasing influence of the vehicle-excited turbulence can be observed. With increasing modulation frequency, a decreasing percentage of modulations related to the oncoming flow is shown. For the analysed case, the turbulence of the oncoming flow dominates the third octave bands and modulation frequencies that are particularly relevant for the human perception. As next step, the developed methodology will be validated under real flow conditions using different vehicles and the active turbulence generator FKFS ***swing***® (see Ref. [66]).

Written by D. Staron: domenic.staron@fkfs.de, *M. Riegel, R. Blumrich, Forschungsinstitut für Kraftfahrwesen und Fahrzeugmotoren Stuttgart (FKFS), Germany*.

8.4. Bibliographic Reviews: bio-inspired aerodynamic noise control and landing gear noise control

In 2019 two useful Bibliographic Reviews were published in areas of interest to aviation aeroacoustics.

As a main contributor to aircraft noise at approach to landing, landing gear noise remains a major research interest amongst aeronautical engineers and aeroacoustic researchers. Numerous technologies have been proposed for the abatement of landing gear noise. “Noise reduction technologies for aircraft landing gear-A bibliographic review” [67], published in Progress in Aerospace Sciences, presents a bibliographical review of such technologies for landing gear noise reduction, taking the Technology Readiness Level (TRL) into consideration. Noise treatment technologies applied directly to the landing gear, such as fairings, but also component optimization, hole coverings, flow blowing and plasma actuators are examples of approaches considered. The associated landing gear wheel bay has also been investigated with liners and leading edge control. Technologies currently at the conceptual design stage or proposed for noise reduction in other engineering fields but which have application potential for landing gears are also assessed.

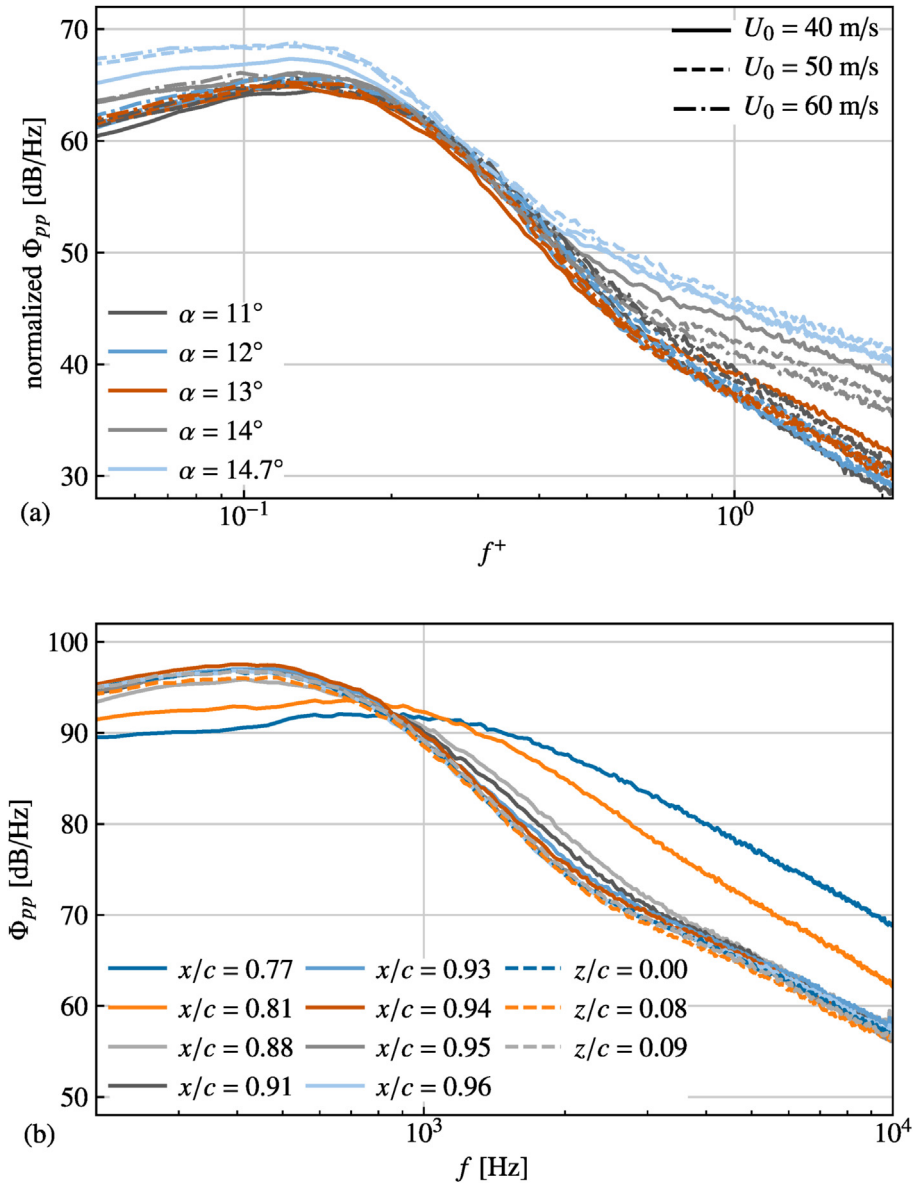

Fig. 43. (a) SPF autospectral power densities measured 13 mm upstream of the trailing-edge scaled according to Refs. [70], (b) streamwise, x/c, and spanwise, z/c, distributions of the SPF autospectral power density at $\alpha = 13^{\circ}$.

It is well-known that many species of owl have the unique ability to fly silently, which can be attributed to their distinctive and special feather adaptations. Inspired therefore by owls, researchers have attempted to reduce the aerodynamic noise of aircraft and other structures using biomimicry. Although fruitful results have been achieved, comparatively little work has been done to summarize the main findings and progresses in this area. In "Bio-Inspired Aerodynamic Noise Control: A Bibliographic Review" [68] a systematic review of the progress and trends of bio-inspired aerodynamic noise control has been conducted including the aerodynamic effects and underlying mechanisms of the four main bio-inspired noise reduction techniques, i.e., leading edge serrations, trailing edge serrations, fringe-type trailing edge extensions and porous material inspired noise reduction.

Both of these papers are published open access.*Written by Gareth J. Bennett:* gareth.bennett@tcd.ie, *School of Engineering, Trinity College Dublin, the University of Dublin, Ireland.*

8.5. Prediction of flow separation noise

Local and intermittent changes in wind speed may induce a higher angle of attack of a wind turbine rotor blade leading to flow separation. The effect of flow separation to the surface pressure fluctuation (SPF) and trailing-edge noise (TEN) was

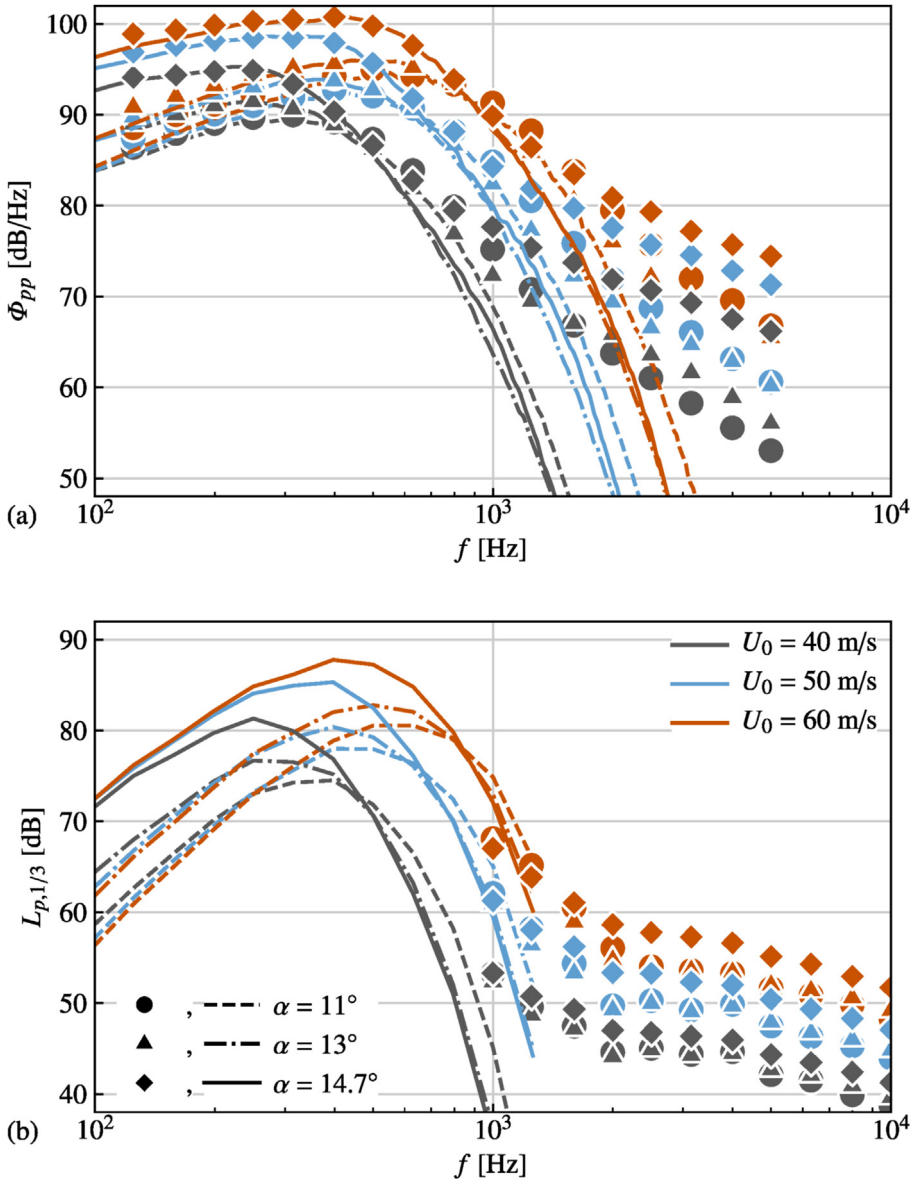

Fig. 44. Comparison of the model and experimental results of (a) autospectral power densities of the SPF and (b) separated flow TEN. For clarity only the one-third octave center frequencies are presented in the measurement results.

measured in the Acoustic Wind-tunnel Braunschweig using a directional microphone and miniature surface pressure sensors. The measurements were conducted using a DU96-W-180 rotor blade profile at pre-stall angles of attack [69]. Because of the limitation of the directional microphone, the maximum sound pressure level at a frequency lower than 1 kHz was not attainable. Therefore, a predictive model of the TEN using the surface pressure fluctuations is needed.

The autospectral power densities of the SPF are self-similar for $f < 2$ kHz for medium angles of attack $11^\circ \leq \alpha \leq 14^\circ$, c. f. figure 43a, and are statistically homogeneous closer to the trailing-edge, c. f. figure 43b [69,70]. A low-order TEN spectrum was estimated using a regression model of the SPF cross-spectral density expressed as Eq. (2) [71], where $\mathcal{R}$ denotes the real part of the cross-spectral density, $\Phi_{pp}(f,\boldsymbol{\xi})$ is the magnitude of the cross-spectral density, $\gamma(f,\boldsymbol{\xi})$ is the coherence function with $\boldsymbol{\xi} = (\xi,\eta)$ is the sensor separation distances in the longitudinal and lateral directions, respectively, and $\Phi_{pp}(f\boldsymbol{x}_0)$ is the autospectral power density nearest to the trailing-edge. Regression models of self-similar functions for $\gamma(f,\xi)$ and $\gamma(f,\eta)$ and a curve fit of $\Phi_{pp}(f\boldsymbol{x}_0)$ are derived in Refs. [71].

$$\mathcal{R}\{\Phi_{pp}(f,\boldsymbol{\xi})\} \approx \Phi_{pp}(f,\boldsymbol{\xi}) = \gamma(f,\boldsymbol{\xi})\Phi_{pp}(f\boldsymbol{x}_0) = \gamma(f,\xi)\gamma(f,\eta)\Phi_{pp}(f\boldsymbol{x}_0) \tag{2}$$

The cross-spectral density at low frequencies compares well against the measured autospectral power densities of the SPF as shown in Fig. 44a. Using Howe's trailing-edge radiation model, the TEN one-third octave band sound pressure levels, $L_{p,1/3}$,

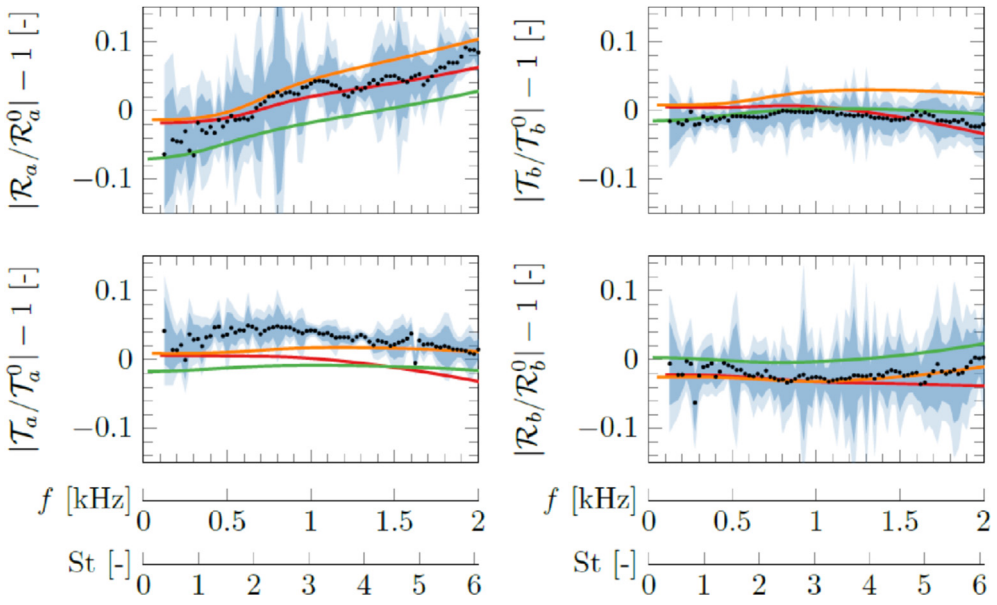

Fig. 45. Measured absolute values (.) of the scattering coefficients for an upstream Mach number of $Ma = 0 : 15$, shown as function of the frequency and Strouhal number together with the 95% and 65% confidence intervals (light blue and blue, respectively). Model results by Aurégan et al. (red), Kooijman et al. (green) and Çınar et al. (orange). (For interpretation of the references to color in this figure legend, the reader is referred to the Web version of this article.)

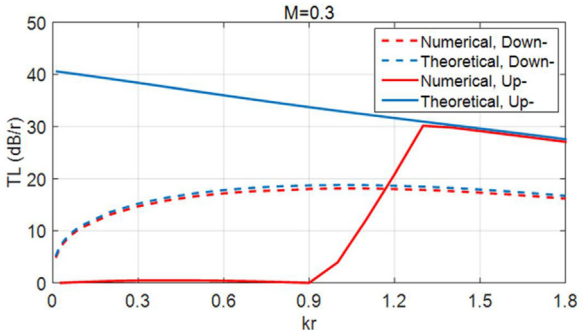

Fig. 46. Damping per duct radius (r) at the Mach-number M = 0.3 in a lined duct as function of the Helmhotz-number kr based on the exact Cremer solution [3]. The theoretical (blue) curves are computed based on the imaginary part of the wave-number corresponding to the exact solution. The red curves are computed based on a FEM solution of the convected wave equation, using the exact Cremer impedance as the wall boundary condition. (For interpretation of the references to color in this figure legend, the reader is referred to the Web version of this article.)

are shown in Fig. 44b. The advantage of using the regression model is that it does not require knowledge of the boundary layer characteristics, unlike Amiet's method [72] or the TNO method [73].

Written by Alexandre Suryadi: alexandre.suryadi@dlr.de, *German Aerospace Center, Braunschweig, Germany*.

8.6. Experimental investigation of the aero-acoustic interaction at an area-expansion

Experimental results on the aero-acoustic interaction at an area expansion are scarce. In this study [74], new experimental data is acquired of the aero-acoustic interaction at an area expansion and compared with recent modelling efforts [75–77]. The aero-acoustic interaction at an area expansion with expansion ratio 0.309 is investigated by measuring the scattering matrix for plane waves at 5 different flow speeds in the incompressible regime. The experimental results are complimented with a comprehensive uncertainty analysis to determine the precision of the data. The scattering coefficients together with derived quantities, such as absorption coefficients and dimensionless end corrections, are compared against recent analytical results. It is shown that there are consistent deviations between the models and measurement results for certain scattering coefficients. The measured end correction on Strouhal number close to the critical value shows a relatively abrupt change. This in comparison with the models, where the change is predicted to be more gradual. Similar observations are made for the absorption coefficient for waves incident upstream of the area expansion, although a qualitative comparison is difficult to make in this case because of the strong influence of the flow downstream of the area-expansion on the results. Fig. 45 shows an example of the results

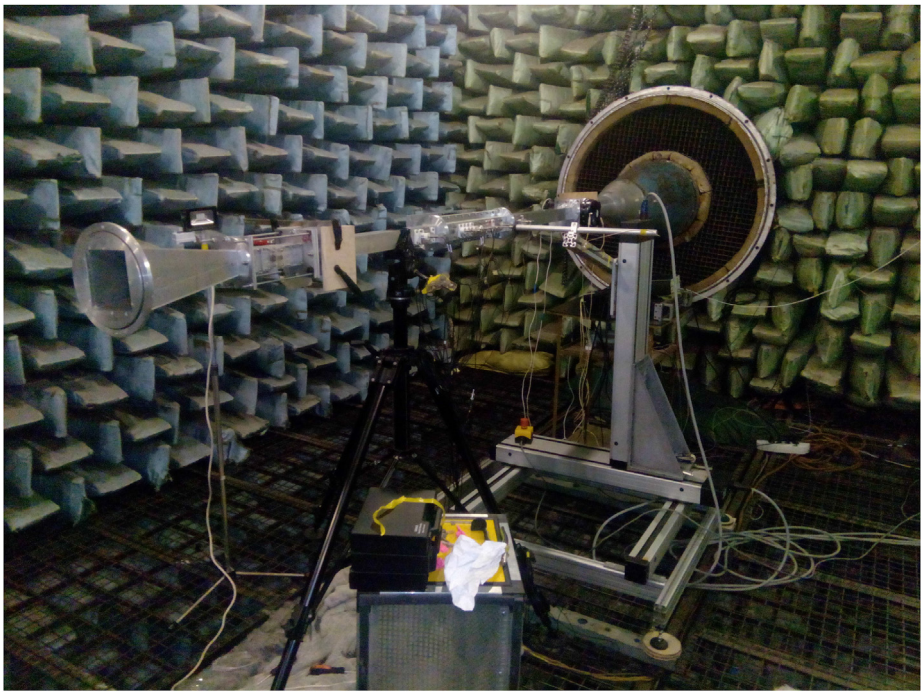

Fig. 47. TsAGI's test rig "Interferometer with the flow" installed in anechoic chamber AC-2.

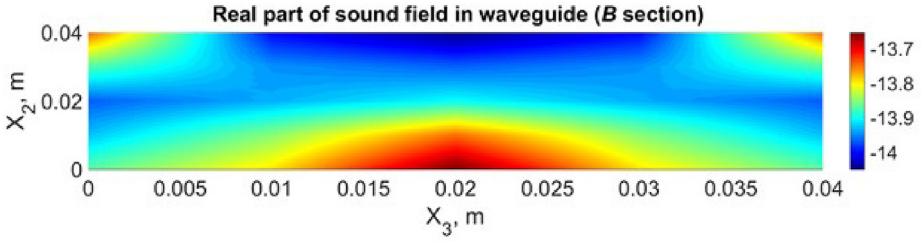

Fig. 48. The sound pressure distribution in the duct section for three-segment liner at M = 0.3 with semi-empirical profile, f = 1000 Hz.

presented as the absolute value of the difference between the scattering matrix and a quasi-steady solution. A database of high quality measurement results [78] has been produced which should be very useful for the further development of accurate models for the acoustic properties of the area expansion.

Written by Luck Peerlings: luck@kth.se, *Susann Boij, Hans Bodén, KTH Royal Institute of Technology, Sweden.*

8.7. Revisiting the Cremer impedance

The 'Cremer impedance' proposed more than half a century ago has been revisited and further developed. The starting point is the solution proposed by Tester 1973 [79] for ducts with a plug flow. This solution assumes well cut-on modes and is not valid for the low and mid-frequency range. In order to remove this limitation the exact Cremer solution has been derived and investigated. The exact solution was first applied to rectangular ducts and substantial improvements compared to Tester's solution were demonstrated and also validated experimentally [80]. However, the exact solution of the Cremer impedance has a negative real part in the low frequency range, indicating that an active boundary is required to provide the maximum damping. Two investigations on the negative resistance have been conducted [81]. First, the 'plug' flow is replaced by a sheared flow by changing the boundary condition and the negative resistance is still found in most cases, demonstrating that the negative resistance is not necessarily an artefact of the boundary condition. Second, since the Cremer impedance is based on mode merging, a mode merging analysis is carried out. This shows that the downstream results are always valid, while some of the upstream results in the low frequency range are invalid in the sense that unexpected mode pairs merge, and the corresponding damping is smaller than expected, see Fig. 46.

Written by Zhe Zhang, Hans Bodén, Mats Åbom: matsabom@kth.se *KTH Royal Institute of Technology, Stockholm, Sweden.*

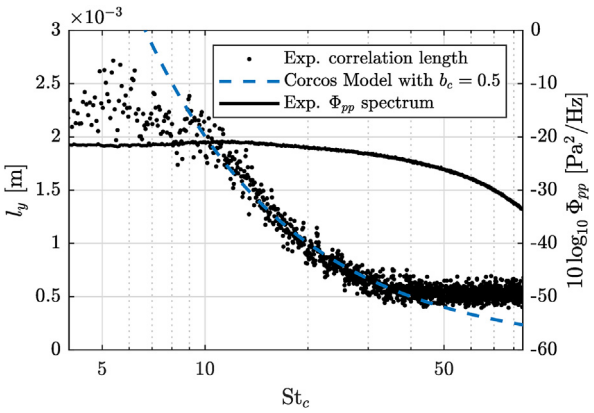

Fig. 49. Measured spanwise correlation length scale l_y and wall pressure spectrum Φ_{pp}.The free-stream Mach number is 0.1 with $Re_c = 700{,}000$ and angle of attack of 0°.

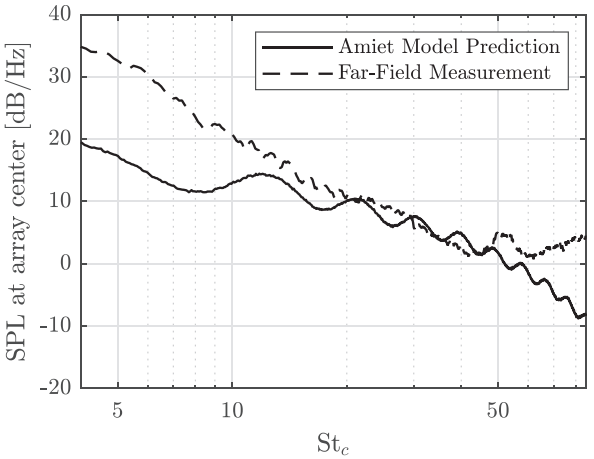

Fig. 50. Comparison of the measured far-field trailing edge noise with the prediction of the Amiet model using the measured surface wall pressure statistics. The SPL levels are based on the source power integration method applied to the conventional beamforming technique. The considered spanwise extend is 0.25 m with M = 0.09, $Re_c = 600{,}000$ and angle of attack of 0°.

8.8. Investigation of sound propagation in rectangular duct with transversally non-uniform flow and anisotropic wall impedance by asymptotic theory and 3D finite element method

Asymptotic theory and 3D Finite Element Method (FEM) are developed for descripting sound propagation in rectangular duct with arbitrary three-dimensional plane-parallel flow at the presence of anisotropic wall impedance [82]. The linearized Euler equations for the main three-dimensional plane-parallel flow with arbitrary velocity profile in duct cross section are considered as a base for constructing mathematical models for sound propagation in the duct. To solve the eigenvalue problem in the case of small Mach number, a version of the singular perturbation theory developed in earlier works of Kopiev and Ostrikov for weakly non-axisymmetric jets [83] is used. The advantage of this method is the ability to describe all types of resonances within the framework of uniformly suitable asymptotic expansions. In this case, the uniform suitability of asymptotic solutions is understood as their applicability regardless of the distance between the eigenvalues of the unperturbed problem, including the cases of their merging (resonances). A 3D Finite Element Method solution based on Galerkin procedure was further developed to describe these effects. The developed asymptotic and numerical approaches were verified and validated for the cases of Mach numbers up to 0.4 at rigid duct walls. TsAGI's test rig "Interferometer with flow" was used not only in the laboratory position, but also was installed in anechoic chamber AC-2 for investigation mean flow profile effects on the sound field structure, see Fig. 47. The developed analytical, numerical and experimental investigations show the strong dependence of sound field in the duct on three-dimensional full velocity profile in the duct cross section that cannot be described by standard 2D approaches, see Fig. 48. The developed approaches are adapted to impedance eduction problem especially for variable-impedance liners.

Written by Nikolay Ostrikov: nikolay.ostrikov@tsagi.ru, *TsAGI, Russia.*

8.9. Unsteady wall pressure measurements using digital MEMS for airfoil trailing edge noise application

Wall pressure fluctuations underneath turbulent boundary layers are a key statistical parameters to measure for airfoil trailing edge noise applications. However, the measurement of these statistics are far from straightforward due to various limitations. Digital micro-electro-mechanical-systems (MEMS) microphones are considered to be a good alternative to the current collection of microphones, overcoming several limitations. One of which is the easy integration of large and high-density arrays due to the relative low costs and small size of digital MEMS microphones, enabling accurate measurement of the space-time turbulence correlations and their amplitudes.

A study was conducted to assess the capability of digital MEMS microphones readily available in the market. For this purpose, the microphones were embedded in a 3D printed NACA0012 airfoil in the open-jet aeroacoustic wind tunnel facility at the University of Twente. Wind tunnel measurements were conducted with flow conditions up to a chord-based Reynolds number of 700,000 associated with a Mach number of 0.1. Far-field measurements were performed using a microphone phased array. In-house beamforming algorithms are applied to determine the far-field noise from the trailing edge.

The wall pressure measurements with the digital MEMS array show promising results. Wall pressure spectra and spanwise correlation length scales were obtained Fig. 49. These measured statistics were used as input for the Amiet Trailing edge noise model [84]. A comparison of the computed far-field radiated noise with the measured far-field noise from the microphone phased array is shown in Fig. 50.

It was demonstrated that digital MEMS microphones can be smoothly integrated in a small area for the application of airfoil trailing edge noise [85]. Improvements to the digital MEMS technology, such as the maximum sound pressure level that they can measure, still need to be made in order to advance the technology for use in higher Mach number flows.

Written by Leandro de Santana: leandro.desantana@utwente.nl, *University of Twente, Netherlands.*

Declaration of competing interest

The authors declare that they have no known competing financial interests or personal relationships that could have appeared to influence the work reported in this paper.

References

[1] A. Rubio Carpio, F. Avallone, D. Ragni, M. Snellen, S. Van Der Zwaag, Mechanisms of broadband noise generation on metal foam edges, Phys. Fluids 31 (2019).
[2] T. Sinnige, B. Della Corte, R. De Vries, F. Avallone, R. Merino-Martnez, D. Ragni, G. Eitelberg, L. Veldhuis, Alleviation of propeller-slipstream-induced unsteady pylon loading by a flow-permeable leading edge, J. Aircraft 56 (2019) 1214–1230.
[3] F. Avallone, L. van den Ende, Q. Li, D. Ragni, D. Casalino, G. Eitelberg, L. Veldhuis, Aerodynamic and aeroacoustic effects of swirl recovery vanes length, J. Aircraft (2019) 1–13.
[4] C. Teruna, D. Ragni, F. Avallone, D. Casalino, A rod-linear cascade model for emulating rotor-stator interaction noise in turbofans: a numerical study, Aero. Sci. Technol. 90 (2019) 275–288.
[5] G. Romani, Q. Ye, F. Avallone, D. Ragni, D. Casalino, Numerical analysis of fan noise for the NOVA boundary-layer ingestion configuration, Aero. Sci. Technol. 96 (2019) 105532.
[6] H. Coanda, Device for Deflecting a Stream of Elastic Fluid into an Elastic Fluid, Patent, 1936. United States, No. 2052869.
[7] M. Pott-Pollenske, K.-C. Pfingsten, Aeroacoustic performance of an airfoil with circulation control, AIAA 2010-3881, in: 16th AIAA/CEAS Aeroacoustics Conference, American Institute of Aeronautics and Astronautics, Stockholm, Sweden, 2010.
[8] L. Rossian, A. Suryadi, K.-S. Rossignol, R. Ewert, M. Herr, J. Delfs, P. Kumar, Numerical and experimental insights into the noise generation of a circulation control airfoil, AIAA 2018-3139, in: 24th AIAA/CEAS Aeroacoustics Conference, American Institute of Aeronautics and Astronautics, Atlanta, Georgia, USA, 2018.
[9] L. Rossian, K.-S. Rossignol, R. Ewert, M. Herr, J. Delfs, Aeroacoustic investigation of a circulation control airfoil, Presentation, in: Presentation at German Aerospace Congress, 2019.
[10] R. Merino-Martinez, E. Neri, M. Snellen, J. Kennedy, D. G. Simons, G.J. Bennett, Comparing flyover noise measurements to fullscale nose landing gear windtunnel experiments for regional aircraft, in: 23rd AIAA/CEAS Aeroacoustics Conference, AIAA 2017-3006, Denver, Colorado, USA.
[11] R. Merino-Martinez, E. Neri, M. Snellen, J. Kennedy, D. G. Simons, G.J. Bennett, Analysis of nose landing gear noise comparing numerical computations, prediction models and flyover and windtunnel measurements, in: 24th AIAA/CEAS Aeroacoustics Conference, AIAA 2018-3139, Atlanta, Georgia, USA.
[12] R. Merino-Martinez, M. Snellen, D.G. Simons, Functional beamforming applied to imaging of flyover noise on landing aircraft, J. Aircraft 53 (2016) 1830–1843.
[13] R. Merino-Martinez, E. Neri, M. Snellen, J. Kennedy, D.G. Simons, G.J. Bennett, Multiapproach study of nose landing gear noise, J. Aircraft (2020), https://doi.org/10.2514/1.C035655 Published Online: 27 Jan 2020.
[14] M. Zaytsev, V. Kopiev, S. Velichko, I. Belyaev, Fly-over noise source localization during acoustic flight tests of advanced passenger aircraft, in: 25th AIAA/CEAS Aeroacoustics Conference, AIAA 2019-2426, Delft, The Netherlands.
[15] V. Kopiev, M. Zaytsev, I. Belyaev, Investigation of airframe noise for a large-scale wing model with high-lift devices, Acoust Phys. 62 (2016) 97–107.
[16] M. Behn, U. Tapken, Investigation of sound generation and transmission effects through the acat1 fan stage using compressed sensing-based mode analysis, in: 25th AIAA/CEAS Aeroacoustics Conference, AIAA 2019-2463, AIAA, Delft, The Netherlands, 2019.
[17] U. Tapken, M. Behn, M. Spitalny, B. Pardowitz, Radial mode breakdown of the acat1 fan broadband noise generation in the bypass duct using a sparse sensor array, in: 25th AIAA/CEAS Aeroacoustics Conference, AIAA 2019-2463, AIAA, Delft, The Netherlands, 2019.
[18] M. Behn, R. Kisler, U. Tapken, Efficient azimuthal mode analysis using compressed sensing, in: 22th AIAA/CEAS Aeroacoustics Conference, AIAA 2016-3038, AIAA, Lyon, France, 2016.
[19] U. Tapken, D. Gutsche, L. Enghardt, Radial mode analysis of broadband noise in flow ducts using a combined axial and azimuthal sensor array, in: 24th AIAA/CEAS Aeroacoustics Conference, AIAA 2018-3139, Atlanta, Georgia, USA.
[20] C. Bogey, On noise generation in low Reynolds number temporal round jets at a Mach number of 0.9, J. Fluid Mech. 859 (2019) 1022–1056.
[21] C. Bogey, P. Pineau, Potential-core closing of temporally developing jets at Mach numbers between 0.3 and 2: scaling and conditional averaging of flow and sound fields, Phys. Rev. Fluid. 4 (2019) 124601.
[22] P. Pineau, C. Bogey, Steepened Mach waves near supersonic jets: study of azimuthal structure and generation process using conditional averages, J. Fluid Mech. 880 (2019) 594–619.

[23] P. Pineau, C. Bogey, Temperature effects on convection speed and steepened waves of temporally developing supersonic jets, AIAAJ. 58 (2020) 1227–1239.
[24] Z.-N.W. Wang, J.C. Tyacke, P.G. Tucker, P. Boehning, Parallel computation of aeroacoustics of industrially relevant complex-geometry aeroengine jets, Comput. Fluid 178 (2019) 166–178.
[25] Z.-N. Wang, J.C. Tyacke, P.G. Tucker, Large eddy simulation of serration effects on an ultra-high-bypass-ratio engine exhaust jet, Compt. Rendus Mec. 346 (2018) 964–977.
[26] A. Di Marco, M. Mancinelli, R. Camussi, Pressure and velocity measurements of an incompressible moderate Reynolds number jet interacting with a tangential flat plate, J. Fluid Mech. 770 (2015) 247–272.
[27] M. Mancinelli, A. Di Marco, R. Camussi, Multivariate and conditioned statistics of velocity and wall pressure fluctuations induced by a jet interacting with a flat plate, J. Fluid Mech. 823 (2017) 134–165.
[28] S. Meloni, A. Di Marco, M. Mancinelli, R. Camussi, Wall-pressure fluctuations induced by a compressible jet flow over a flat plate at different Mach numbers, Exp. Fluid 60 (2019).
[29] J. Yin, M. Barbarino, H. Brouwer, G. Reboul, M. Gennaretti, G. Bernardini, C. Testa, L. Vigevano, Helicopter Fuselage Scattering Effects for Exterior/interior Noise Reduction, Technical Report Terms of Reference for the GARTEUR Action Group HC/AG-24, DLR, CIRA, NLR, ONERA, Roma TRE University, CNR-INSEAN, Politecnico di Milano, 2015.
[30] J. Yin, K.-S. Rossignol, M. Barbarino, D. Bianco, C. Testa, H. Brouwer, R. Janssen, G. Reboul, L. Vigevano, G. Bernardini, M. Gennaretti, J. Serafini, C. Poggi, Garteur activities on acoustical methods and experiments for studying on acoustic scattering, CEAS Aeronaut. J. 10 (2019) 531–551.
[31] D. J. B. F. Rossignol, K.-S., On the relevance of convection effects for a laser-generated sound source, in: 21th AIAA/CEAS Aeroacoustics Conference, AIAA 2015-3146, Dallas, Texas, USA.
[32] M. Lummer, C. Richtery, C. Prber, J. Delfs, Validation of a model for open rotor noise predictions and calculation of shielding effects using a fast bem, in: 19th AIAA/CEAS Aeroacoustics Conference, AIAA 2013-2096, Berlin, Deutschland.
[33] J. Yin, Investigation of rotor noise shielding effects by the helicopter fuselage in forward flight, J. Aircraft 56 (2019) 1–12.
[34] F. Errico, M. Ichchou, S. De Rosa, O. Bareille, F. Franco, The modelling of the flow-induced vibrations of periodic flat and axial-symmetric structures with a wave-based method, J. Sound Vib. 424 (2018) 32–47.
[35] F. Errico, M. Ichchou, F. Franco, S. De Rosa, O. Bareille, C. Droz, Schemes for the sound transmission of flat, curved and axisymmetric structures excited by aerodynamic and acoustic sources, J. Sound Vib. 476 (2019) 221–238.
[36] F. Errico, G. Tufano, O. Robin, N. Guenfoud, M. Ichchou, N. Atalla, Simulating the sound transmission loss of complex curved panels with attached noise control materials using periodic cell wavemodes, Appl. Acoust. 156 (2019) 21–28.
[37] G. Petrone, G. Melillo, A. Laudiero, S.D. Rosa, A statistical energy analysis (sea) model of a fuselage section for the prediction of the internal sound pressure level (spl) at cruise flight conditions, Aero. Sci. Technol. 88 (2019) 340–349.
[38] N. Hu, C. Appel, S. Haxter, S. Callsen, A. Klabes, Simulation of wall pressure fluctuations on an airbus-a320 fuselage in cruise flight condition, in: 25th AIAA/CEAS Aeroacoustics Conference, AIAA 2019-2728, Delft, The Netherlands.
[39] N. Hu, N. Reiche, R. Ewert, Simulation of turbulent boundary layer wall pressure fluctuations via Poisson equation and synthetic turbulence, J. Fluid Mech. 826 (2017) 421–454.
[40] A. Klabes, C. Appel, M. Herr, M. Bouhaj, Fuselage excitation during cruise flight conditions: measurement and prediction of pressure point spectra, in: 21st AIAA/CEAS Aeroacoustics Conference, AIAA 2015-3115, Dallas, Texas, USA.
[41] S. Haxter, C. Spehr, Comparison of model predictions for coherence length to in-flight measurements at cruise conditions, J. Sound Vib. 390 (2017) 86–117.
[42] D. A. Smith, A. Filippone, N. Bojdo, A parametric study of counter rotating open rotor noise, in: 25th AIAA/CEAS Aeroacoustics Conference Downloaded, AIAA 2019-2400, Delft, The Netherlands.
[43] J. Biesheuvel, M. Tuinstra, L.D. de Santana, K. Venner, Effect of turbulent boundary layer induced coherence loss on beamforming measurements in industrial scale wind tunnel tests, in: 25th AIAA/CEAS Aeroacoustics Conference, AIAA 2019-2463, AIAA, Delft, The Netherlands, 2019.
[44] S. A. Rizzi, Toward reduced aircraft community noise impact via a perception-influenced design approach, in: InterNoise 2016, 45th International Congress and Exposition of Noise Control Engineering, Hamburg, Germany.
[45] R. Pieren, L. Bertsch, D. Lauper, B. Schaffer, Improving future low-noise aircraft technologies using experimental perception-based evaluation of synthetic flyovers, Sci. Total Environ. 692 (2019) 68–81.
[46] L. Bertsch, F. Wolters, W. Heinze, M. Pott-Pollenske, J. Blinstrub, System noise assessment of a tube-and-wing aircraft with geared turbofan engines, J. Aircraft 56 (2019) 1577–1596.
[47] C. Testa, C. Poggi, G. Bernardini, M. Gennaretti, Pressure-field permeable-surface integral formulations for sound scattered by moving bodies, J. Sound Vib. 459 (2019) 114860.
[48] M. Gennaretti, G. Bernardini, C. Poggi, C. Testa, Velocity-potential boundary-field integral formulation for sound scattered by moving bodies, AIAAJ. 56 (2018) 3547–3557.
[49] K. M. Schoder, S., Helmholtz's decomposition applied to aeroacoustics, in: 25th AIAA/CEAS Aeroacoustics Conference, AIAA 2019-2561, Delft, The Netherlands.
[50] M. Kaltenbacher, Numerical Simulation of Mechatronic Sensors and Actuators: Finite Elements for Computational Multiphysics, Springer Berlin Heidelberg, 2015.
[51] S. Schoder, Aeroacoustic Analogies Based on Compressible Flow Data, PhD Thesis, TU Wien, 2019.
[52] U. Kowarsch, C. hrle, M. Keler, E. Krämer, Aeroacoustic simulation of a complete H145 helicopter in descent flight, J. Am. Helicopter Soc. 61 (2016) 1–13.
[53] L. Drrwchter, M. Keler, E. Krämer, Numerical assessment of open-rotor noise shielding with a coupled approach, AIAAJ. 57 (2019) 1930–1940.
[54] E.R. Busch, M.S. Wurst, M. Keler, E. Krämer, Computational aeroacoustics with higher order methods, in: W.E. Nagel, D.H. Kroner, M.M. Resch (Eds.), High Performance Computing in Science and Engineering 12, Springer Verlag, 2013.
[55] L. Dürrwächter, M. Keßler, E. Krämer, Numerical assessment of CROR noise shielding with a coupled Mhring analogy and BEM approach, in: 24th AIAA/CEAS Aeroacoustics Conference, AIAA 2018-2822, Atlanta, Georgia, USA.
[56] M. Howe, A review of the theory of trailing edge noise, J. Sound Vib. 6 (1978) 437–465.
[57] P. Bernicke, R. Akkermans, V. Ananthan, R. Ewert, J. Dierke, L. Rossian, A zonal noise prediction method for trailing-edge noise with a porous model, Int. J. Heat Fluid Flow 80 (2019) 108469.
[58] M. Herr, R. Ewert, C. Rautmann, M. Kamruzzaman, D. Bekiropoulos, R. Arina, A. Iob, P. Batten, S. Chakravarthy, F. Bertagnolio, Broadband trailing-edge noise predictions: overview of banc-iii results, in: 21st AIAA/CEAS Aeroacoustics Conference, AIAA 2015-2847, Dallas, Texas, USA.
[59] M. Herr, K. Rossignol, J. Delfs, N. Lippitz, M. Moessner, Specification of porous materials for low-noise trailing-edge applications, in: 20st AIAA/CEAS Aeroacoustics Conference, AIAA 2014-3041, Atlanta, Georgia, USA.
[60] R. Roncen, E. Piot, F. Mery, Bayesian inference for modal identification in ducts with a shear flow, J. Acoust. Soc. Am. 146 (2019).
[61] A. Dawi, R. Akkermans, Direct noise computation of a generic vehicle model using a finite volume method, Comput. Fluid 191 (2019) 104243.
[62] A. Dawi, R. Akkermans, Direct and integral noise computation of two square cylinders in tandem arrangement, J. Sound Vib. 436 (2018) 138–154.
[63] A. Dawi, R. Akkermans, Spurious noise in direct noise computation with a finite volume method for automotive applications, Int. J. Heat Fluid Flow 72 (2018) 243–256.
[64] N. Oettle, The Effects of Unsteady On-Road Flow Conditions on Cabin Noise, Ph.D. thesis, Durham University, UK, 2013.
[65] D. Staron, M. Riegel, R. Blumrich, J. Wiedemann, Einfluss turbulenter anstrmung und fahrzeugerregter turbulenz auf das windgerusch im fahrzeug, in: Fortschritte der Akustik DAGA 2019, Deutsche Gesellschaft fr Akustik e.V., Rostock, Germany, 2019, pp. 161–164.
[66] M. Riegel, R. Blumrich, M. Helfer, New technology for unsteady wind noise measurements in an aeroacoustic full-scale wind tunnel, in: International Conference on Vehicle Aerodynamics 2016: Aerodynamics by Design, Institution of Mechanical Engineers, Coventry, UK, 2016, pp. 45–56.
[67] K. Zhao, P. Okolo, E. Neri, P. Chen, J. Kennedy, G.J. Bennett, Noise reduction technologies for aircraft landing gear-A bibliographic review, Prog. Aero. Sci. 112 (2019) 100589.

[68] Y. Wang, K. Zhao, X.-Y. Lu, Y.-B. Song, G.J. Bennett, Bio-inspired aerodynamic noise control: a bibliographic review, Appl. Sci. 9 (2019) 2224.
[69] A. Suryadi, M. Herr, Wall pressure spectra on a DU96-W-180 profile from low to pre-stall angles of attack, in: 21st AIAA/CEAS Aeroacoustics Conference, AIAA 2015-2688, Dallas, Texas, USA.
[70] A. Suryadi, Kinematic and acoustic similarities of separated turbulent boundary layers, AIAAJ. 57 (2019) 2435–2446.
[71] A. Suryadi, Prediction of trailing-edge noise for separated turbulent boundary layers, 27 September, in: A. Dillmann, G. Heller, E. Kramer, C. Wagner, C. Tropea, S. Jakirlic (Eds.), New Results in Numerical and Experimental Fluid Mechanics XII, Volume 142 of Notes on Numerical Fluid Mechanics and Multidisciplinary Design, Springer, 2019, pp. 769–779.
[72] R.K. Amiet, Acoustic radiation from an airfoil in a turbulent stream, J. Sound Vib. 41 (1975) 407–420.
[73] R. Parchen, Progress Report DRAW: A Prediction Scheme for Trailing-Edge Noise Based on Detailed Boundary Layer Characteristics, Technical Report TNO report HAG-RPT-980023, TNO Institute of Applied Sciences, The Netherlands, 1998.
[74] L. Peerlings, S. Boij, H. Bodén, Experimental investigation of the aero-acoustic interaction at an area-expansion, J. Sound Vib. 457 (2019) 197–211.
[75] Y. Aurégan, A. Debray, R. Starobinski, Low frequency sound propagation in a coaxial cylindrical duct: application to sudden area expansions and to dissipative silencers, J. Sound Vib. 243 (2001) 461–473.
[76] G. Koijman, A. Hirschberg, Y. Aurégab, Influence of mean flow and geometrical ratio on scattering of sound at a sudden area expansion in a duct, J. Sound Vib. 329 (2010) 607–626.
[77] O.Y. Cinar, S. Boij, G. Cinar, B. Nilsson, Sudden area expansion in ducts with flow a comparison between cylindrical and rectangular modelling, J. Sound Vib. 396 (2017) 307–324.
[78] L. Peerlings, Measured Scattering and Absorption Coefficients of an Area Expansion with Flow, DiVA, 2019, Version 1.0.
[79] B.J. Tester, The propagation and attenuation of sound in lined ducts containing uniform or plug flow, J. Sound Vib. 28 (1973) 151–203.
[80] Z. Zhang, H. Tiikoja, L. Peerlings, M. Abom, Experimental analysis on the exact cremer impedance in rectangular ducts, SAE 2018-01-1523, in: SAE Technical Paper, SAE, 2018.
[81] Z. Zhang, H. Bodn, M. Abom, The cremer impedance: an investigation of the low frequency behavior, J. Sound Vib. 459 (2019).
[82] N. Ostrikov, S. Denisov, M. Yakovets, M. Ipatov, Investigation of sound propagation in rectangular duct with transversally non-uniform flow and anisotropic wall impedance by asymptotic theory and 3D finite element method, in: 25th AIAA/CEAS Aeroacoustics Conference, AIAA 2019-2640, Delft, The Netherlands.
[83] V. Kopiev, N. Ostrikov, S. Chernyshev, J. Elliott, Aeroacoustics of supersonic jet issued from corrugated nozzle: new approach and prospects, Int. J. Aeroacoustics 3 (2004) 199–228.
[84] R. Amiet, Noise due to turbulent flow past a trailing edge, J. Sound Vib. 47 (1976) 387–393.
[85] M.P. Sanders, L.D. de Santana, M. Azarpeyvand, C.H. Venner, Unsteady surface pressure measurements on trailing edge serrations based on digital mems microphones, in: AIAA/CEAS Aeroacoustics Conference, AIAA 2018-3290, Atlanta (USA), 2018.